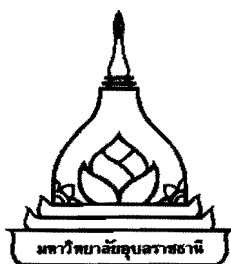


**MONTE CARLO SIMULATION ON THE EFFECT OF AIR
MASS ABOVE THE PRINCESS SIRINDHORN NEUTRON
MONITOR TO ATMOSPHERIC NEUTRONS
FROM COSMIC RAYS**

DUMRONGSAK RODPHOTHONG

**A THESIS SUBMITTED IN PARTIAL FULFILLMENT OF THE REQUIREMENTS
FOR THE DEGREE OF MASTER OF SCIENCE
MAJOR IN PHYSICS
FACULTY OF SCIENCE
UBON RATCHATHANI UNIVERSITY
YEAR 2012
COPYRIGHT OF UBON RATCHATHANI UNIVERSITY**



**การจำลองผลกระทบของมวลอากาศเหนือสถานีตรวจวัดนิวตรอนสิรินธร
ต่ออนุภาคนิวตรอนในบรรยากาศจากรังสีคอสมิกโดยวิธีมอนติคาร์โล**

ดำรงศักดิ์ รอดโพธิ์ทอง

วิทยานิพนธ์นี้เป็นส่วนหนึ่งของการศึกษาตามหลักสูตรปริญญาวิทยาศาสตรมหาบัณฑิต

สาขาวิชาฟิสิกส์ คณะวิทยาศาสตร์

มหาวิทยาลัยอุบลราชธานี

พ.ศ. 2555

ลิขสิทธิ์นี้เป็นของมหาวิทยาลัยอุบลราชธานี



THESIS APPROVAL
UBON RATCHATHANI UNIVERSITY
MASTER OF SCIENCE
MAJOR IN PHYSICS FACULTY OF SCIENCE

TITLE MONTE CARLO SIMULATION ON THE EFFECT OF AIR MASS ABOVE THE
PRINCESS SIRINDHORN NEUTRON MONITOR TO ATMOSPHERIC
NEUTRONS FROM COSMIC RAYS

NAME MR.DUMRONGSAK RODPHOTHONG

THIS THESIS HAS BEEN ACCEPTED BY

.....*Tanin Nutaro*..... CHAIR
(ASST.PROF.DR.TANIN NUTARO)

.....*Chanruangrit Channok*..... COMMITTEE
(ASST.PROF.DR.CHANRUANGRIT CHANNOK)

.....*Nipon Gasiprong*..... COMMITTEE
(ASST.PROF.DR.NIPON GASIPRONG)

.....*Janpen Intaraprasert*..... DEAN
(ASST.PROF.DR.JANPEN INTARAPRASERT)

APPROVAL BY UBON RATCHATHANI UNIVERSITY

.....*Utith Inprasit*.....
(ASSOC.PROF.DR.UTITH INPRASIT)

VICE PRESIDENT FOR ACADEMIC AFFAIRS

FOR THE PRESIDENT OF UBON RATCHATHANI UNIVERSITY

ACADEMIC YEAR 2012

ACKNOWLEDGEMENT

I would like to thank my advisor, Asst. Prof. Dr. Tanin Nutaro for his instructions, valuable advisement and improvement, not only this thesis, but for the researches and project since I was in first year undergrad. I appreciate his patience, suggestions and supporting during the part year of developing this thesis.

I would like to thank Dr. Alejandro Sáiz for his valuable advice, suggestions, support and techniques for using LINUX and FLUKA programming. Special thanks for my Mom, Dad and brother for their cheerfulness, love, care and all support they gave to me.

Finally, I would like to thank the people who gave me suggestions, cheerfulness, support and companionship during the time I developed this thesis.

Dumrongrak
(Mr.Dumrongsak Rodphothong)
Researcher

บทคัดย่อ

ชื่อเรื่อง : การจำลองผลกระทบของมวลอากาศเหนือสถานีตรวจวัดนิวตรอนสิรินธร
ต่ออนุภาคนิวตรอนในบรรยากาศจากรังสีคอสมิกโดยวิธีมอนติคาร์โล

โดย : คำรงค์ดี โพธิ์ทอง

ชื่อปริญญา : วิทยาศาสตรมหาบัณฑิต

สาขาวิชา : ฟิสิกส์

ประธานกรรมการที่ปรึกษา : ผู้ช่วยศาสตราจารย์ ดร. ธาณินทร์ นุตโร

ศัพท์สำคัญ : สถานีตรวจวัดนิวตรอน การจำลองแบบมอนติคาร์โล
โปรแกรมฟลาคา รังสีคอสมิก

สถานีตรวจวัดอนุภาคนิวตรอนเป็นกุญแจที่สำคัญ สำหรับการศึกษการเปลี่ยนแปลงตามเวลาของรังสีคอสมิกที่มาจากภายนอกกาแล็กซี โดยเฉพาะอย่างยิ่งที่เกี่ยวข้องกับผลกระทบที่มาจากดวงอาทิตย์ เครื่องตรวจวัดรังสีคอสมิกที่อยู่ภายในชั้นบรรยากาศของโลกนั้น ไม่สามารถที่จะบันทึกปริมาณอนุภาครังสีคอสมิกได้โดยตรง เนื่องจากอนุภาคที่เรียกว่ารังสีคอสมิกปฐมภูมิจะเกิดอันตรกิริยากับนิวเคลียสในชั้นบรรยากาศทำให้เกิดเป็นอนุภาคทุติยภูมิขึ้นมา ซึ่งสถานีตรวจวัดนิวตรอนสามารถทำการตรวจวัดและบันทึกปริมาณของอนุภาคนิวตรอนทุติยภูมิที่มาจากการแตกตัวในชั้นบรรยากาศนี้ได้ สถานีตรวจวัดนิวตรอนสิรินธรถูกติดตั้งในบริเวณที่มีค่ารังสีคอสมิกสูงถึง 16.8 กิกะโวลต์ ซึ่งทำให้ได้ข้อมูลใหม่ที่แสดงความสัมพันธ์ระหว่างพลังงานของอนุภาคกับการเปลี่ยนแปลงของปริมาณรังสีในขณะที่ดวงอาทิตย์กำลังหมุนรอบตัวเอง แอนไอโซโทปของรังสีคอสมิก การลดแบบฟอร์บ์ และการเปลี่ยนแปลงตามวัฏจักรของดวงอาทิตย์ สำหรับงานวิจัยนี้เราได้ใช้วิธีการจำลองแบบมอนติคาร์โล โดยได้จำลองผลกระทบจากโครงสร้างชั้นบรรยากาศที่มีต่อปริมาณอนุภาคนิวตรอนทุติยภูมิเหนือสถานีตรวจวัดนิวตรอนสิรินธรโดยใช้โปรแกรมฟลาคา ซึ่งทำให้เข้าใจในกระบวนการที่เกิดขึ้นในชั้นบรรยากาศได้ดี อีกทั้งจะทำให้ทราบการตอบสนองของระบบวัดต่ออนุภาคนิวตรอนทุติยภูมิ ในการศึกษาทำให้ทราบข้อมูลและวิธีการเพื่อการวิเคราะห์ในขั้นต่อไป และมีความเข้าใจที่ดีขึ้นในผลกระทบดังกล่าว

ABSTRACT

TITLE : MONTE CARLO SIMULATION ON THE EFFECT OF AIR MASS
ABOVE THE PRINCESS SIRINDHORN NEUTRONS MONITOR TO
ATMOSPHERIC NEUTRONS FROM COSMIC RAYS
BY : DUMRONGSAK RODPHOTHONG
DEGREE : MASTER OF SCIENCE
MAJOR : PHYSICS
CHAIR : ASST.PROF. TANIN NUTARO, Ph.D.

KEYWORDS : NEUTRON MONITOR / MONTE CARLO SIMULATION /
FLUKA / COSMIC RAYS

Neutron monitors are recognized as a key tool for studying the time variations of galactic cosmic rays, especially with regard to solar effects. Cosmic-ray detectors inside the atmosphere do not record cosmic ray particles directly. The so-called primary cosmic rays interact with nuclei in the atmosphere to produce secondary daughter products. Neutron monitors record predominantly the secondary neutrons from these atmospheric showers. The Princess Sirindhorn Neutron Monitor (PSNM) was installed at a high vertical cutoff rigidity of 16.8 GV. It provides unique data on the energy dependence of solar synodic variations, cosmic ray anisotropy, Forbush decreases, and solar modulation. In this work we performed Monte Carlo simulations of the atmospheric structure effects on secondary neutron counts above The Princess Sirindhorn Neutron Monitor by using the FLUKA program. These atmospheric processes are well understood, and the response of neutron monitors to these secondary particles is simulated. This work also provides the techniques for further analysis and a better understanding of those effects.

CONTENTS

	PAGE
ACKNOWLEDGEMENT	I
THAI ABSTRACT	II
ENGLISH ABSTRACT	III
LIST OF TABLES	VII
LIST OF FIGURES	VIII
CHAPTER	
1 INTRODUCTION	
1.1 Overview	1
1.2 Motivation	3
1.3 Objectives	3
1.4 Outline of the thesis	3
2 A BRIFF INTRODUCTION TO THE COSMIC RAYS	
2.1 What are Cosmic Rays	4
2.2 Discover and Early Research	4
2.3 How cosmic rays are detected	6
2.4 Primary spectra and Composition	8
2.5 Atmospheric cascade	9
2.6 Solar energetic particles	13
2.7 Solar effects on cosmic ray variations	14
2.8 Cutoff rigidity	15
2.9 Neutron monitors	15
3 THE PRINCESS SIRINDHORN NEUTRONS MONITOR	
3.1 History	19
3.2 Installation	20
3.3 Data acquisition	21

CONTENTS (CONTINUE)

	PAGE
4 NUMERICAL METHODS	
4.1 Monte Carlo methods	24
4.2 What is FLUKA	25
4.3 FLUKA's physics, structure and capabilities	26
5 MODELING OF ATMOSPHERIC CASCADES	
5.1 Model Standard atmosphere	32
5.2 Geometry and materials	34
5.3 Source particles	36
5.4 Readout setting	39
5.5 Programming	39
6 RESULTS AND DISCUSSION	
6.1 Atmospheric cascade	45
6.2 Calculation of neutron flux	47
6.3 Including a mountain of rock (granite)	49
REFERENCES	51
APPENDICES	
A MODEL OF ATMOSPHERIC PROPERTIES	55
B PRESSURE AND DENSITY EQUATIONS	64
VITAE	68

LIST OF TABLES

TABLES	PAGE
5.1 The U.S. Standard Atmosphere altitude profile	33
5.2 The U.S. Standard Atmosphere composition	33
5.3 Properties of our layers for Monte Carlo modeling	37
5.4 The molecular composition of granite	38
5.5 Atomic composition of the granite at 2565 m for the mountain	38
A.1 Values in the FLUKA input file “AtmosphereInf.txt”	57

LIST OF FIGURES

FIGURES	PAGE
1.1 The Princess Sirindhorn Neutron Monitor (PSNM)	2
2.1 The balloon flight of Victor Hess	5
2.2 A variety of ways to detect cosmic rays	7
2.3 Data from the Princess Sirindhorn Neutron Monitor	7
2.4 The cosmic ray spectrum	8
2.5 Atmospheric cascade	10
2.6 The energy spectrum of secondary neutrons at sea level	11
2.7 The sunspot cycle	13
2.8 Forbush Decrease	14
2.9 The magnetic cutoff rigidity around the world	16
2.10 The IGY neutron monitor	17
2.11 Components of an NM64 neutron monitor	17
2.12 The neutron monitor and bare counters at Doi Inthanon	18
2.13 Simulation of the interactions caused in a neutron monitor	18
3.1 The PSNM station logo	20
3.2 The Princess Sirindhorn Neutron Monitor building	21
3.3 The 18 counter tubes and 3 bare counters inside the PSNM	22
3.4 In the proportional counter	23
3.5 The main window of the neutron monitor data	23
5.1 The atmospheric model including 100 layers of the atmosphere	35
5.2 The diagram of the process of the FLUKA simulation	44
6.1 Atmospheric cascade from 5 mono-energetic 1GeV primary protons	45
6.2 Atmospheric cascade form 5 primary protons which energy 10 GeV	46
6.3 The cascades from 17, 20 and 30 GeV primary protons	46
6.4 Show a more realistic simulation when we take the effect of rock	47
6.5 Secondary neutron flux with dry air	48

LIST OF FIGURES (CONTINUE)

FIGURES	PAGE
6.6 Histogram of the flux of neutrons	49
6.7 Histogram of the flux of neutrons, as generated by John Clem	50

CHAPTER 1

INTRODUCTION

1.1 Overview

Cosmic rays are energetic particles or gamma rays from outer space. The most commonly detected primary cosmic rays are protons (87%), alpha particles (12%), ions of other elements, and electrons (Pomerantz, 1971). They move along the interplanetary magnetic field to Earth. When a cosmic ray strikes an air molecule in earth's atmosphere, it can produce a cascade of secondary particles. Which we can detect them by using a neutron monitor.

The Princess Sirindhon Neutron Monitor (PSNM), the first neutron monitor station in Thailand, shown in Figure 1.1. It was set up at Doi Inthanon in Chiang Mai province in order to measure the count rate of secondary neutron, which is related to the flux of cosmic rays in space. Doi Inthanon is the highest point of Thailand. This is important because the secondary neutrons are absorbed by the atmosphere. At Doi Inthanon, the count rate is about 6 times higher than that at sea level. When cosmic rays enter the earth magnetic field, some of them with lower energy will move along the Earth's magnetic field to near a magnetic pole. Cosmic ray with a higher energy will pass through the magnetic field. We use the cutoff rigidity, a momentum per charge, to separate the cosmic rays by their rigidity thresholds for penetration of the cosmic rays through Earth's geomagnetic field to the atmosphere, in units of GV (GV stands for giga Volt). The cutoff rigidity of Thailand is 16.8 GV, which the highest cutoff rigidity of any neutron monitor station in the world.

Since most cosmic rays are charged particles of high energy, they can cause damage to electronic equipment above Earth's atmosphere, such as in satellites, aircraft, etc., affecting communication and causing effects on the genetic structure of organisms. This provides motivation to support the study of cosmic rays and to try to protect expensive equipment from cosmic rays.

To understand the ground-based neutron monitor (NM) as a primary particle detector a relationship between the count rate and primary flux must be established. Primary particles enter the atmosphere and undergo multiple interactions resulting in showers of secondary particles which may reach ground level and be detected by NM. A yield function must incorporate the propagation of particle through the earth's atmosphere and the detection response of a NM to

secondary particles such as neutrons, protons, muons and pions. The yield function S related to the NM count rate N and E as the kinetic energy can be described by formula (Clem, 2000):

$$N(E_n) = \int_{E_c} S(E_n, E_p) j(E_p) dp \quad (1.1)$$

Where

- E_p the kinetic energy of the primary proton;
- E_n the kinetic energy of the secondary neutron;
- E_c the vertical cutoff rigidity;
- j the Galactic cosmic ray flux.

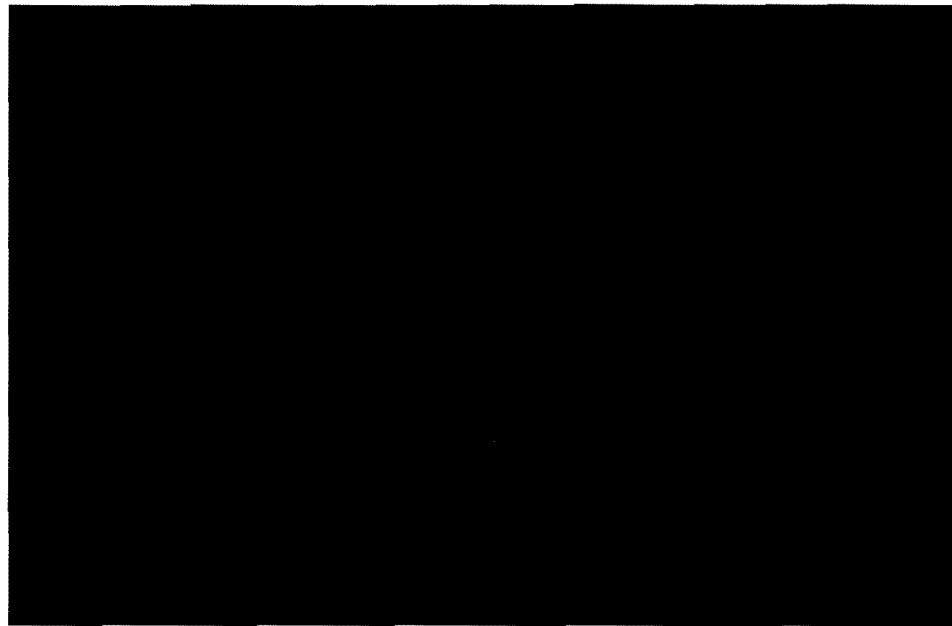


Figure 1.1 The Princess Sirindhorn Neutron Monitor building at Doi Inthanon, Chiang Mai, Thailand.

In order to simulate secondary cosmic ray we use the FLUKA program, a software package to simulate particle transport and interactions with matter based on the Monte Carlo method. We model the interaction of primary cosmic rays in Earth's atmosphere examine the yield function at Doi Inthanon, which will allows us to better understand the flux of primary cosmic rays at Doi Inthanon.

1.2 Motivation

The PSNM is the first neutron monitor station in Thailand, which has the highest cutoff rigidity in the world, and we can measure data that have never been observed from anywhere else in the world. This work is about simulation processing for advanced analysis about cosmic rays at the PSNM by using FLUKA simulations to better understand the detector.

1.3 Objectives

1.3.1 To study the Monte Carlo simulation by using FLUKA program.

1.3.2 To model the atmospheric structure, and use the FLUKA program to study effects of the atmospheric structure on the secondary neutron counts as detected by the PSNM.

1.3.3 Find the yield function and calculate the expected neutron flux at Doi Inthanon's altitude of 2,565 meters.

1.4 Outline of the thesis

This thesis consists of six chapters and two appendices. The first chapter overviews the work and the basic ideas of the research. The research motivations are mentioned here.

The fundamental and relevant background knowledge on cosmic rays, the Earth's atmosphere, and neutron monitor are given in Chapter 2, starting with the cosmic rays in space. The measurements and the structure of a neutron monitor, will be described. In addition, the standard atmospheric composition is discussed.

In Chapter 3, the history and the installation of PSNM are explained, including the data acquisition.

We then describe short summary of FLUKA, the program for calculations of particle transport and interactions with matter based on Monte Carlo simulations, in Chapter 4.

For the atmospheric simulations, we will explain the modeling of atmospheric structures and processes of the FLUKA program in Chapter 5, and the conclusions are included in the last chapter.

Finally, two appendices will show information regarding each layer of the atmosphere for the FLUKA modeling, including the altitude, pressure, temperature, density and chemical composition, and a derivation of the pressure equation, respectively.

CHAPTER 2

A BRIEF INTRODUCTION TO THE COSMIC RAYS

2.1 What are Cosmic Rays

Cosmic rays are high energy charged particles, originating in outer space, that travel at nearly the speed of light and strike the earth from all directions. Most cosmic rays are the nuclei of atoms, ranging from the lightest to the heaviest elements in the periodic table. Cosmic rays also include high energy electrons, positrons, and other subatomic particles. The term “cosmic rays” usually refers to galactic cosmic rays, which originate in sources outside the solar system, distributed throughout our Milky Way galaxy. However, this term has also come to include other classes of energetic particles in space, including nuclei and electrons accelerated in association with energetic events on the Sun (called solar energetic particles), and particles accelerated in interplanetary space.

2.2 Discover and Early Research

In 1912 Victor Hess made measurements of radiation levels at different altitudes with electroscopes aboard a balloon (Shown in Figure 2.1). The motivation for this study was to distance the electroscopes from radiation sources in the Earth. Hess went as high as 17,500 feet in his balloon without oxygen tanks. Surprisingly, he found that the radiation levels increased with altitude. Hess interpreted this result to mean that radiation is entering the atmosphere from outer space (Hess, 1912). Hess received the Nobel Prize in Physics in 1936 for his discovery. In the 1920s the term “cosmic rays” was coined by Robert Millikan who made measurements of ionization due to cosmic rays from deep under water to high altitudes and around the globe. Millikan believed that his measurements proved that the primary cosmic rays were gamma rays, i.e., energetic photons. And he proposed a theory that they were produced in interstellar space as by-products of the fusion of hydrogen atoms into the heavier elements, and that secondary electrons were produced in the atmosphere by Compton scattering of gamma rays. But then, in 1927, a Dutch physicist, J. Clay found evidence (Clay, 1927) of a variation of cosmic ray intensity with latitude, which indicated that the primary cosmic rays are deflected by the geomagnetic field.



Figure 2.1 Left: The balloon flight of Victor Hess. Right: Victor Hess before his balloon flight, during which he observed cosmic ray intensity increasing with altitude.

and must therefore be charged particles, not photons. In 1929, Bothe and Kolhörster (1929) discovered charged cosmic-ray particles that could penetrate 4.1 cm of gold. Charged particles of such high energy could not possibly be produced by photons from Millikan's interstellar fusion process. In 1930, Bruno Rossi (1930) predicted a difference between the intensities of cosmic rays arriving from the east and the west that depends upon the charge of the primary particles the so called "east-west effect". Three independent experiments (Johnson, 1934; Alvarez, 1934; Rossi, 1934a) found that the intensity is, in fact, greater from the west, proving that most primaries are positive. During the years from 1930 to 1945, a wide variety of investigations confirmed that the primary cosmic rays are mostly protons, and the secondary radiation produced in the atmosphere is primarily electrons, photons and muons. In 1948, observations with nuclear emulsions carried by balloons to near the top of the atmosphere (Frier et al., 1948; Bradt & Peters, 1948) showed that approximately 10% of the primaries are helium nuclei (alpha particles) and 1% are heavier nuclei of the elements such as carbon, iron, and lead. During a test of his equipment for measuring the east-west effect, Rossi observed that the rate of near-simultaneous discharges of two widely separated Geiger counters was larger than the expected accidental rate. In his report on the experiment, Rossi (1934b) wrote "it seems that once in a while the recording equipment is struck by very extensive showers of particles, which causes coincidences between the counters, even placed at large distances from one another". In 1937 Pierre Auger, unaware of Rossi's earlier report, detected the same phenomenon and investigated it in some detail. He concluded that

high-energy primary cosmic-ray particles interact with air nuclei high in the atmosphere, initiating a cascade of secondary interactions that ultimately yield a shower of electrons, and photons that reach ground level.

Soviet physicist Sergey Vernov was the first to use radiosondes to perform cosmic ray readings with an instrument carried to high altitude by a balloon. On April 1, 1935, he took measurements at heights up to 13.6 kilometers using a pair of Geiger counters in an anti-coincidence circuit to avoid counting secondary ray showers.

Homi J. Bhabha derived an expression for the probability of scattering positrons by electrons, a process now known as Bhabha scattering. His classic paper, jointly with Walter Heitler, published in 1937 described how primary cosmic rays from space interact with the upper atmosphere to produce particles observed at the ground level. Bhabha and Heitler explained the cosmic ray shower formation by the cascade production of gamma rays and positive and negative electron pairs.

2.3 How cosmic rays are detected

From the 1930s to the 1950s, before man-made particle accelerators reached very high energies, cosmic rays served as a source of particles for high energy physics investigations, and led to the discovery of subatomic particles that included the positron and muon. Although these applications continue, since the dawn of the space age the main focus of cosmic ray research has been directed towards astrophysical investigations of where cosmic rays originate, how they get accelerated to such high velocities, what role they play in the dynamics of the Galaxy, and what their composition tell us about matter from outside the solar system. To measure cosmic rays directly, before they have been slowed down and broken up by the atmosphere, research is carried out by instruments carried on spacecraft and high altitude balloons, using particle detectors similar to those used in nuclear and high energy physics experiments. Cosmic ray are studied in a variety of ways depending on how much energy they have. This is illustrated in figure 2.2.

The lowest energy cosmic rays are absorbed in the upper atmosphere and they can only be detected by equipment on board satellites and high altitude balloons. In Thailand we measure the flux of neutrons using a ground based detector called a Neutron Monitor (NM), which will be explained in the next section. Figure 2.3 shows an example of the count rate of the Princess Sirindhorn Neutron Monitor at Doi Inthanon, which varies with a one-day period due to rotation of the Earth.

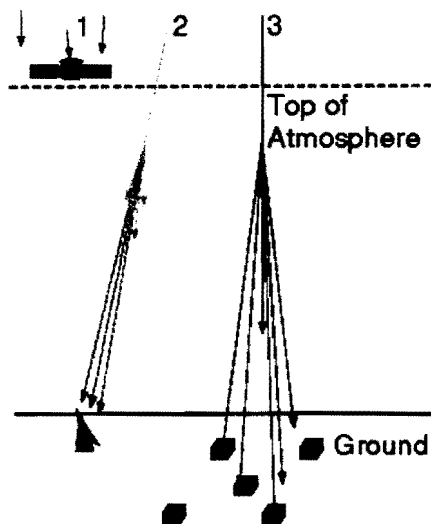


Figure 2.2 A variety of ways to detect cosmic rays

1. Low energy cosmic rays detected by instruments carried in satellites.
2. Higher energy cosmic rays generate a small air shower. The Cerenkov radiation emitted by the shower is detected by a large telescope on ground.
3. Even higher energy cosmic rays very big air shower. The particle in the shower travel to the ground where they can be recorded by an array of detector.

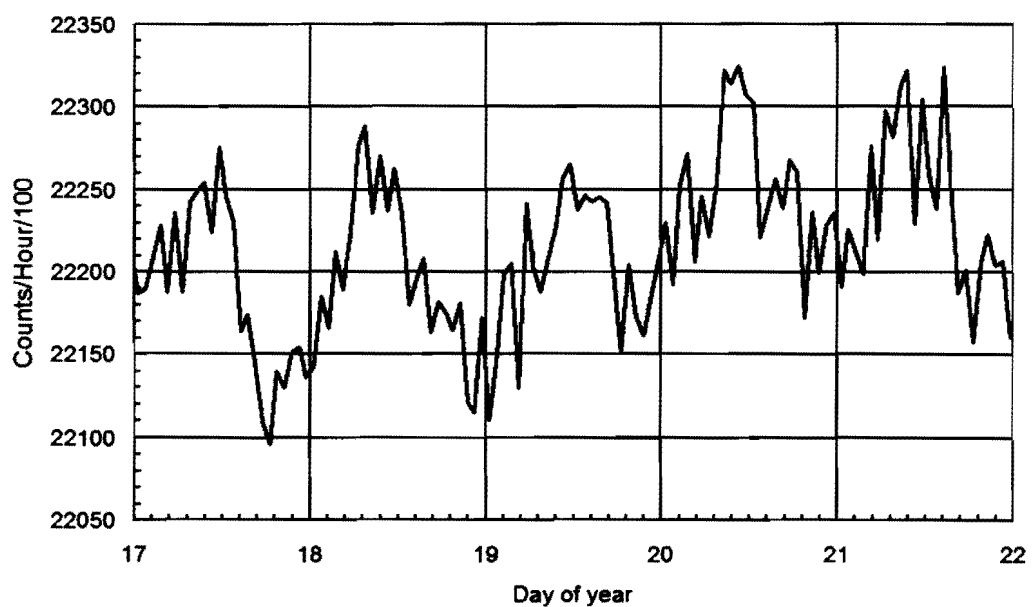


Figure 2.3. Some data from the Princess Sirindhorn Neutron Monitor in January, 2011

2.4 Primary spectra and Composition

The range of energies encompassed by cosmic rays is truly enormous, starting at about 10^7 eV and reaching 10^{20} eV for the most energetic cosmic ray ever detected. By plotting this range of energies against the number of cosmic rays detected at each energy we generate a cosmic ray spectrum which clearly shows that the number of cosmic rays drop off dramatically as we go to higher energies. (See in figure 2.4)

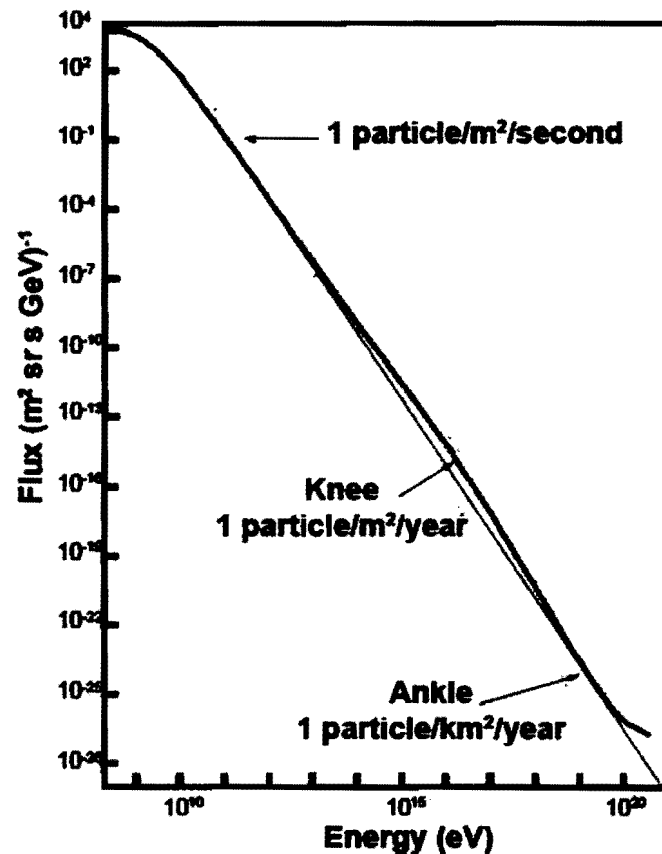


Figure 2.4 The cosmic ray spectrum clearly shows that the number of cosmic rays (the cosmic ray flux) detected drops off dramatically as we go to higher energies. The spectrum exhibits a 'knee' and an 'ankle', both of which deviate from the standard exponential decline (blue line).

Roughly speaking, for every 10% increase in energy beyond 10^9 eV, the number of cosmic rays per unit area falls by a factor of 1,000. However, if we look at the spectrum more closely we can see a knee at $\sim 10^{15}$ eV and an ankle at $\sim 10^{18}$ eV. (Shellard, 2001)

The origin of these changes in the steepness of the spectrum is still the subject of intense study, but it is assumed that they distinguish between populations of cosmic rays originating via different mechanisms. Current suggestions are that the cosmic rays with energies less than about 10^{10} eV are primarily solar cosmic rays produced in solar flares and coronal mass ejections, while those with energies between 10^{10} eV and the knee at 10^{15} eV are galactic cosmic rays produced in the shocks of supernova remnants. The origin of the cosmic rays with energies between the knee and ankle is unclear. They are again thought to be produced within the Galaxy, but the energies are too high for them to be accelerated by the shocks of supernova remnants. The origin for the ultra-high energy cosmic rays below the ankle is also a mystery, but many have suggested that these may be created outside of our Galaxy.

At the top of the Earth's atmosphere the cosmic rays are largely composed of protons (87%) and α -particles (12%). A small contribution of heavier nuclei ($\sim 1\%$). Upon entering the Earth's atmosphere these primary cosmic rays produce secondary cosmic rays in interactions with the atoms in air.

2.5 Atmospheric cascade

When higher energy cosmic rays hit the upper atmosphere (about 20 km up) they lose about half of their energy by creating a jet of particles which carries on travelling in almost the same direction as the cosmic rays. The particles in the jet can themselves create more particles as they hit other nuclei of oxygen or nitrogen in the air. This jet is called an extensive air shower and keeps on growing until the particles in the shower run out of energy and are absorbed in the atmosphere see in Figure 2.5. We refer to the initial particle that starts the shower as the primary cosmic rays. The particles created in the air shower are known as secondary cosmic rays. Over a million of the secondary particles which are produced when primary cosmic rays hit the atmosphere pass right through your body every minute.

2.5.1 The nucleonic component

The high energies of the primary cosmic rays are well in excess of the binding energies of atomic nuclei (typically 7–9 MeV per nucleon). Consequently, the predominant nuclear reaction in the atmosphere is that of spallation. In these reactions, nucleons are sputtered off the target nucleus. Spallation-produced nucleons largely maintain the direction of the impacting particle and go on inducing spallation in other target nuclides, producing a nuclear cascade in the Earth's atmosphere (Figure 2.5). Because neutrons do not suffer ionization losses as do protons,

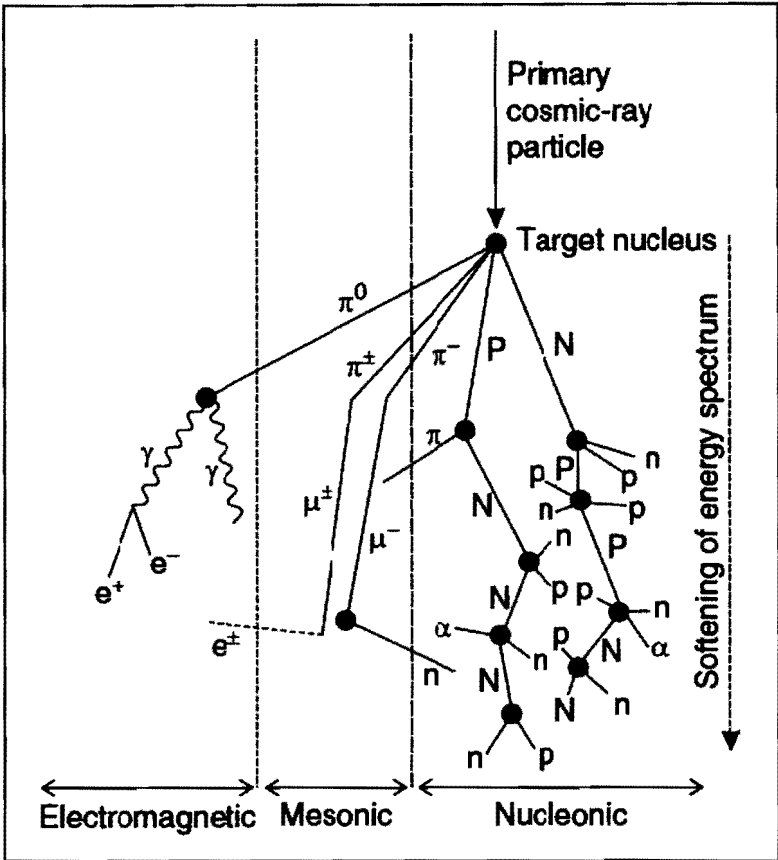


Figure 2.5 The secondary cosmic ray cascade in the atmosphere. Abbreviations used: n, neutron, p, proton (capital letters for particles carrying the nuclear cascade), α , alpha particle, e^{\pm} , electron or positron, γ , gamma-ray photon, π , pion, μ , muon. (Tibor, 2010)

the composition of the cosmic-ray flux changes from proton-dominated to neutron-dominated in the course of the nuclear cascade. At sea level, neutrons constitute 98% of the nucleonic cosmic-ray flux. Another change in the character of the cosmic rays on their way through the atmosphere is that the energy of the secondary neutrons is significantly lower than that of primaries. At ground level, energies > 10 GeV are, for the purpose of Earth-science applications, absent. The neutron energy spectrum has peaks around 100 MeV, 1–10 MeV and < 1 eV (Figure 2.6). The relative shape of the > 1 MeV peaks is invariant between sea-level and high-mountain altitude. The spectrum only changes at much higher elevations, on approaching 12 km. (Tibor, 2010)

2.5.2 Flavours of neutron energy

High-energy neutrons are capable of producing spallation reactions.

They have energies ranging from 10 GeV down to about 10 MeV. High-energy neutrons are

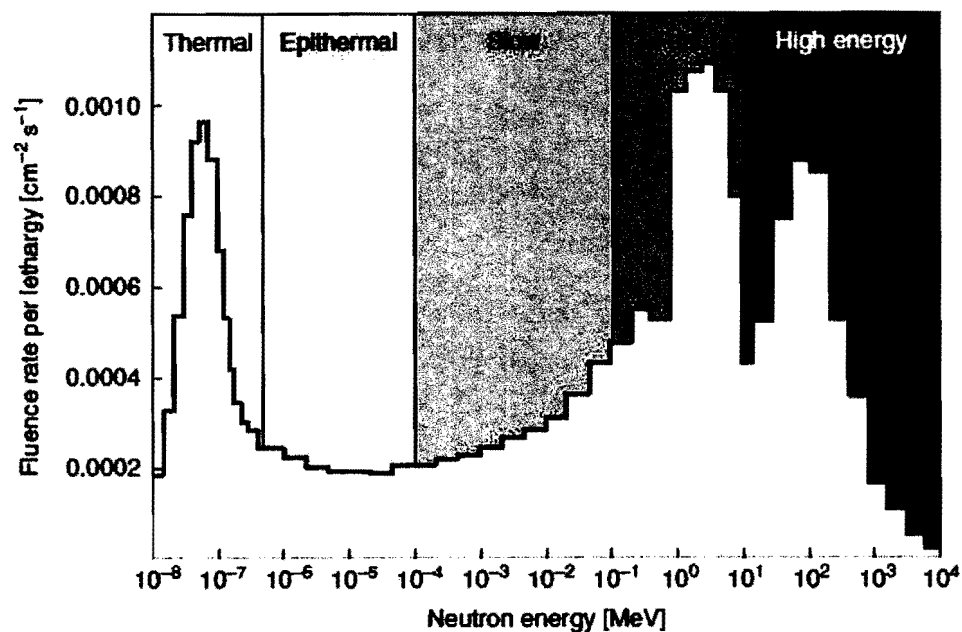


Figure 2.6 The energy spectrum of secondary cosmic ray neutrons at sea level (Goldhagen, et al., 2002). Lethargy is the natural logarithm of energy.

themselves the result of spallation reactions, and are the main carrier of the nuclear cascade. Fast neutrons, 0.1–10 MeV, have insufficient energy to induce spallation reactions. However, they may induce some evaporation reactions, e.g. energetically favourable (n, α) reactions.

Fast neutrons are themselves products of nuclear evaporation: a de-excitation process named by analogy to molecules evaporating from the surface of a heated liquid. Evaporation reactions can be induced by any particle interaction supplying sufficient separation energy.

Slow Neutrons, 100 eV and 100 keV, are produced continuously, as fast neutrons lose energy through elastic and inelastic collisions with nuclei; this process is called moderation.

Epithermal neutrons are produced by further moderation (0.5–100 eV).

Finally, **thermal neutrons** have achieved energy equilibrium with their surroundings; their mean energy at environmental temperatures is ~ 0.025 eV.

There is no generally accepted convention on the classification of neutrons. The energy ranges defined here for the purpose of this thesis are customary in cosmic-ray physics; other fields, such as nuclear engineering, use different classifications.

2.5.3 The mesonic component

Collisions of high-energy primary cosmic rays with atomic nuclei high in the atmosphere produce mesons. These are mostly pions, which decay within a short distance (a few metres) predominantly to muons (μ^\pm) (Figure 2.5). The production of the latter in this decay process is being proved by the fact that the conservation of momentum demands that the process be a two particle decay. The sign of the charge is being conserved in the decay process which can be written: (Sandstrom, 1965)

$$\pi^\pm \longrightarrow \mu^\pm + \nu. \quad (2.1)$$

Muons belong to the particle family of leptons and can be considered as the heavier brother of the electron (206.7 times heavier). They have a half-life of 2.2 μ s. At the speed of light this would give them a range, before they decay, of only 660 m. However, at relativistic speeds, the lifetime of the muon, as we perceive it, is much longer. Due to this time-dilation effect of special relativity, muons can reach the Earth's surface. Muons (μ^-) decay into an electron, an electronantineutrino, and a muon-neutrino. Antimuons (μ^+) decay to a positron, an electron-neutrino, and a muon-antineutrino. This process follows the scheme:

$$\mu^\pm \longrightarrow e^\pm + 2\nu. \quad (2.2)$$

Muons are produced high in the atmosphere (typically 15km) and lose about 2GeV to ionization before reaching the ground. Their energy and angular distribution reflect a convolution of production-energy-spectrum, energy loss in the atmosphere and decay. For example, 2.4 GeV muons have a decay length of 15 km, which is reduced to 8.7km by energy loss. The mean energy of muons at sea level is ~ 4 GeV. Muons (and other particles) of this energy level are generated within a cone-shaped shower, with all particles staying within about 1 degree of the primary particle's path. Because muons interact only weakly with matter (mostly via ionization) they have a much longer range than nucleons, and therefore are the most abundant cosmic-ray particles at sea level. However the nucleonic component dominates cosmogenic nuclide production at the Earth's surface. Muons, in turn, dominate production at depth in the subsurface.

2.5.4 Electromagnetic component

At the Earth’s surface, the electromagnetic component consists of electrons, positrons and photons, primarily from electromagnetic cascades initiated by decay of neutral and charged mesons (Figure 2.5). Muon decay is the dominant source of low-energy electrons at sea level. The electromagnetic component is not relevant for the Earth science applications covered in this thesis and is therefore not considered further.

2.6 Solar energetic particles

Solar energetic particles (SEPs) are high-energy particles from the Sun. SEPs are accelerated by explosions at the Sun called solar storms at the active regions, i.e., sunspot groups. The frequency of SEP events correlates with the number of sunspots, which rises and falls approximately every 11 years as shown in Figure 2.7.

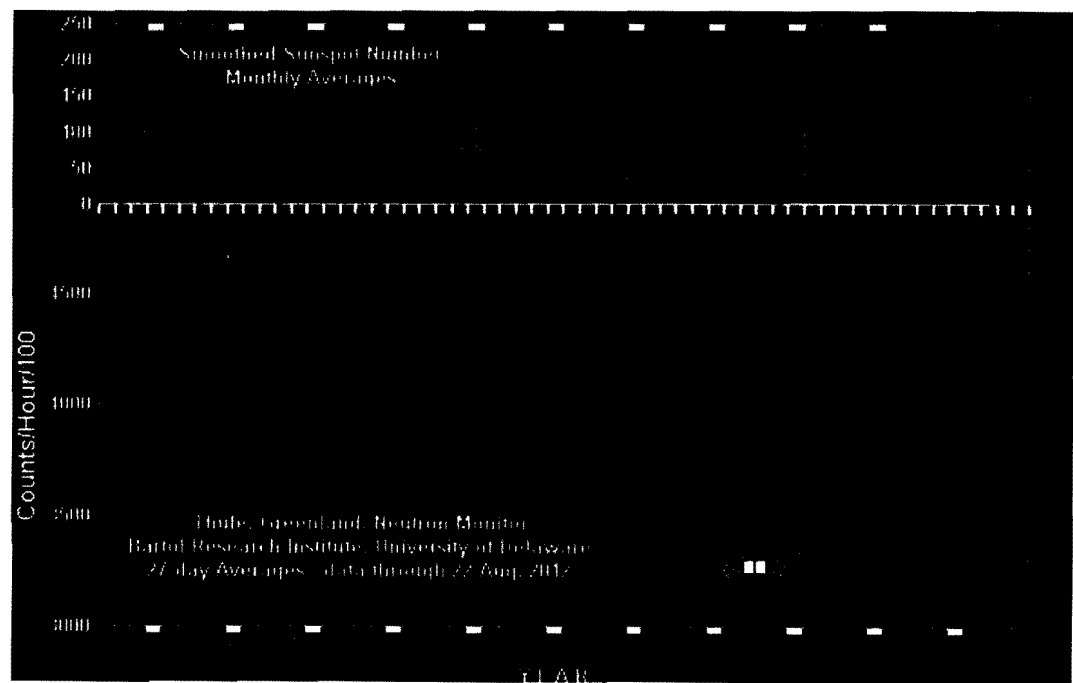


Figure 2.7 The sunspot cycle, with peaks approximately every 11 years. The next solar maximum will occur during 2012-2014. Note that the GCR flux is generally lower when the sunspot number is higher.

When sunspots are present, solar flares and Coronal Mass Ejection (CMEs) are produced and accelerate solar particles to high energy. The solar flares can be classified into two types: impulsive flares and gradual flares. Impulsive flares involve explosive energy released in the form of thermal energy and can accelerate particles to high energies from ~ 10 MeV to ~ 1 GeV. Nuclear reactions of energetic protons at the Sun can produce solar neutrons that come to the Earth. Gradual flares involve explosive energy released in the forms of both thermal energy, giving rise to the flare, and kinetic energy, giving rise to a CME. In a gradual event, most escaping SEP ions are accelerated by shock waves associated with the CME with up to ~ 10 GeV of energy, corresponding to 99% of the speed of light for protons. The SEP composition is mostly the same as the Sun's.

2.7 Solar effects on cosmic ray variations

Galactic cosmic rays (GCRs) normally come to the Earth from all directions and at all times. Because the Earth is often influenced by the Sun, the Sun also has effects on the GCRs. There are changes in the flux of GCRs when the Sun produces CMEs, in which a strong solar magnetic field moves out toward the Earth and inhibits the inward transport of GCRs. Such an event is known as a Forbush decrease. After that the GCRs intensity will recover back to normal over the next several days as shown in Figure2.8.

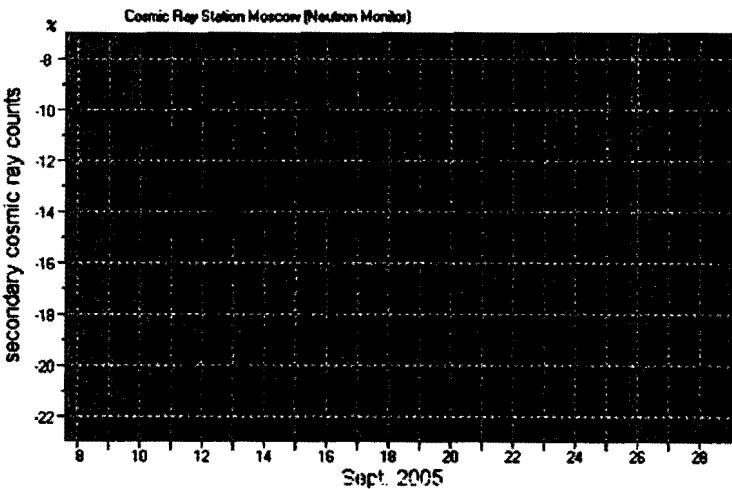


Figure 2.8 Forbush decrease event in September, 2005 as recorded by the Moscow neutron monitor station (science.nasa., 2005)

2.8 Cutoff rigidity

2.8.1 Magnetic cutoff rigidity

The primary cosmic rays move along the interplanetary magnetic field and Earth's magnetic field to enter Earth's atmosphere. The Earth's magnetic field is a bubble of magnetism that surrounds the Earth and protects us from sub-GeV cosmic rays. At the equator, the horizontal magnetic field is stronger than at the poles. Thus the ability of cosmic rays to reach Earth's atmosphere depends on the latitude and longitude. The lower limit in rigidity for cosmic rays to pass through the magnetic field to arrive vertically above a given location at Earth is called the geomagnetic vertical cutoff rigidity. This is calculated in units of momentum per charge (GV) according to

$$P_c = \frac{pc}{q}, \quad (2.3)$$

where P_c is the vertical cutoff rigidity, p is the momentum in GeV/c, c is the velocity of light, and q is the particle charge. In Figure 2.9 we see that Thailand has the maximum magnetic cutoff rigidity in the world. The vertical cutoff rigidity at Doi Inthanon is 16.8 GV. This means that charged particles with a rigidity below this value cannot reach the atmosphere above Doi Inthanon. However, there are cosmic rays of higher rigidity in outer space that can arrive there.

2.8.2 Atmospheric cutoff rigidity

After the primary cosmic rays pass through the Earth's magnetic field, they strike air molecules (mainly nitrogen molecules) at the top of atmosphere and produce many more particles called secondary cosmic rays. Some particles are absorbed by the atmosphere, but if primary has sufficient energy, some secondaries can arrive at the ground. Typically a primary cosmic ray must have a rigidity of at least 1 GV to yield a detectable flux of particles (e.g., neutrons) at sea level so this value is called the atmospheric cutoff.

2.9 Neutron monitors

The first neutron monitors were used in the US and Peru to study geomagnetic effects. The first worldwide network of neutron monitors used the IGY (International Geophysical Year, 1957) design (see Figure 2.10), similar to the design used by John Simpson for the first neutron monitor in 1948.

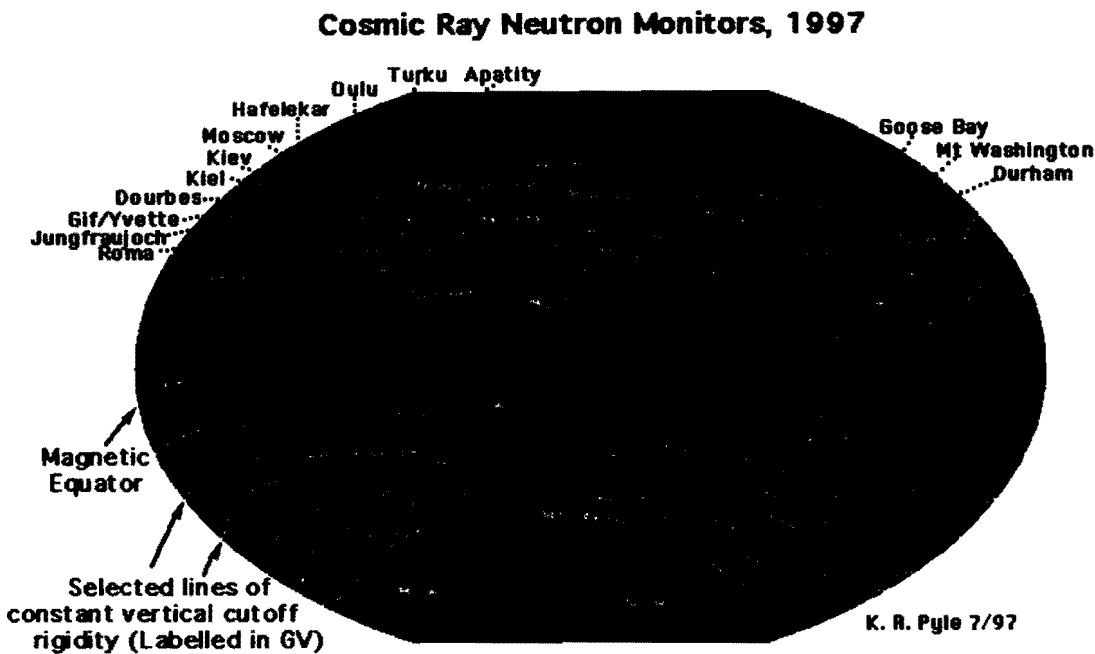


Figure 2.9 The magnetic cutoff rigidity around the world along with some neutron monitor locations. Note the maximum at Thailand. (Image credit: Pyle, K. R.)

The components of the IGY monitor are a neutron sensitive proportional tube, surrounded by a paraffin moderator material and a lead target. The functions of these components will be described shortly below. In 1957-1958, 50 IGY monitor stations were installed at different locations around the world.

After that, in 1964, a new generation of neutron monitors was developed, with the NM64 design (see Figure 2.11 and Figure 2.12), which gives a higher counting rate than the IGY design. An important component of the original NM64 design is a $^{10}\text{B F}_3$ (boron trifluoride) gas proportional counter to yield nuclear reactions between ^{10}B and neutrons to produce Li and He nuclei:



(Nowadays the $^{10}\text{BF}_3$ counter may be replaced by a ^3He counter.) The product nuclei can be detected in the proportional counter. The lead producer can produce more neutrons when atmospheric neutrons impact Pb nuclei. There is a 3-inch polyethylene reflector surrounding the monitor to trap neutrons inside and to protect against disturbance by thermal particles from

outside. There is also a polyethylene moderator surrounding each tube, which serves to reduce (moderate) the neutron energy, which increases the probability of neutron interactions in the ^{10}B F_3 gas (see Figure 2.13). A Bare Counter is a counter with a moderator, i.e., an NM64 with no reflector or lead producer.

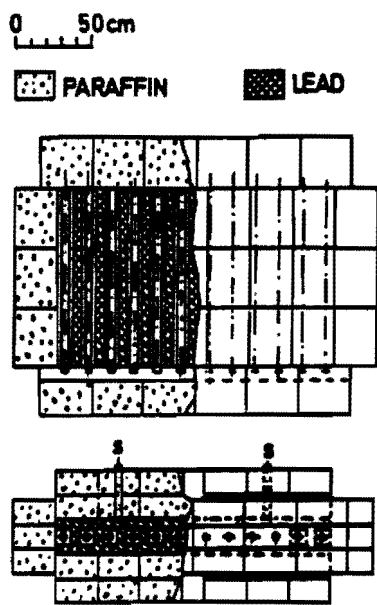


Figure 2.10 The IGY neutron monitor (Simpson, 1957)

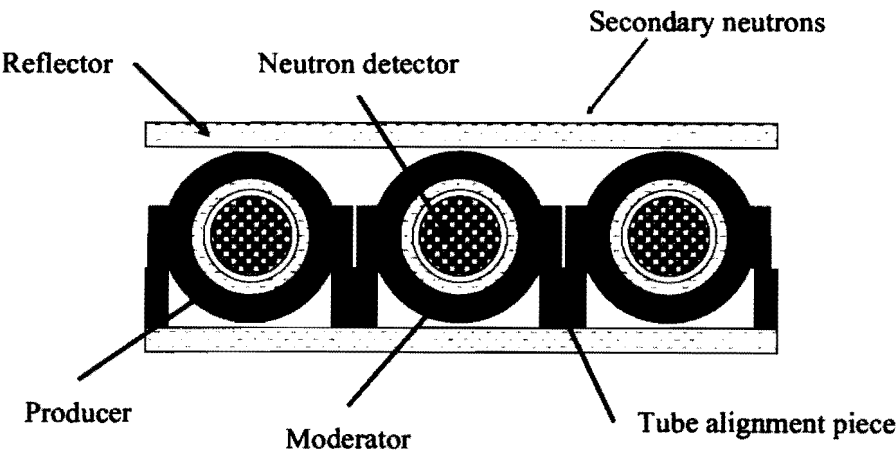


Figure 2.11 Components of an NM64 neutron monitor



Figure 2.12 The neutron monitor and bare counters at Doi Inthanon

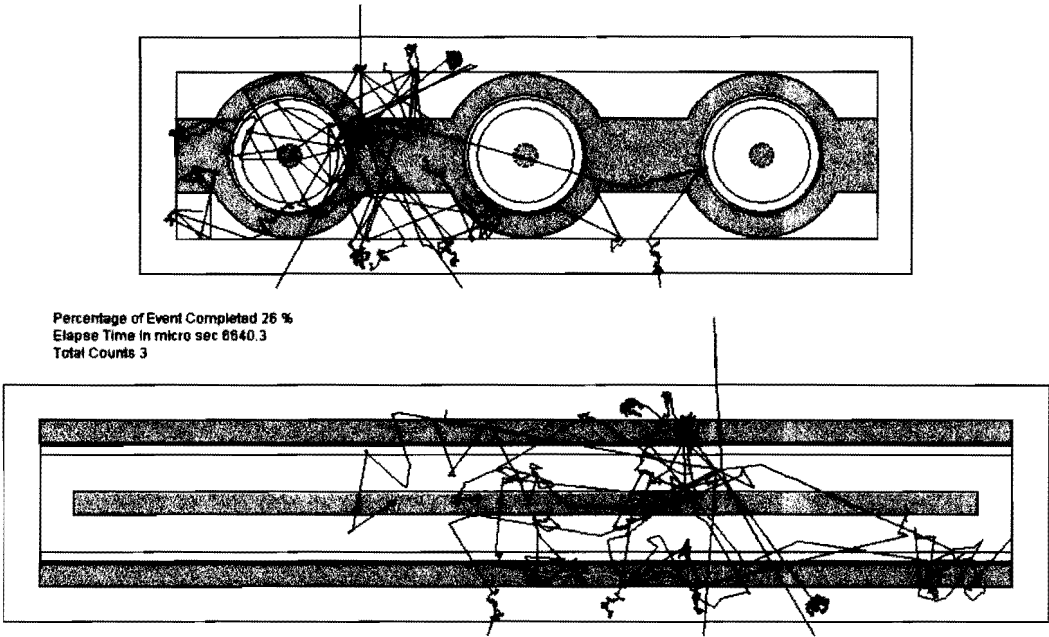


Figure 2.13 Simulation of the interactions caused by an atmospheric secondary neutron in a neutron monitor. The lines are the tracks of neutrons. The blue lines are for neutrons above 2 MeV, green lines are for neutrons between 1 keV and 2 MeV, and red lines are for neutrons below 1 keV. (Image credit: John Clem)

CHAPTER 3

THE PRINCESS SIRINDHORN NEUTRONS MONITOR

3.1 History

HRH Princess Sirindhorn graciously gave her permission for a neutron monitor station at Doi Inthanon, Thailand's highest mountain, to be called the "Princess Sirindhorn Neutron Monitor" (PSNM). PSNM measures the flux of cosmic rays from space that collide with the atmosphere above Doi Inthanon. Neutron monitor stations have been set up at various locations around the world in order to study the cosmic rays from space for a long time (Figure 2.9). Thailand is in a unique location, at the Earth's magnetic equator and close to the offset dipole center. Here the Earth's horizontal magnetic field is strongest, and only relatively high-energy (or high-rigidity) particles can penetrate the field. PSNM is the fixed neutron monitor station located at the world's highest magnetic cutoff rigidity (16.8 GV) (see Figure 2.9). Doi Inthanon is the highest mountain in Thailand 2565 m and the reduced atmospheric absorption leads to a count rate that is 6 times higher than at sea level, yielding greatly improved statistics. Thus the measurements provide useful and unique scientific information. With a standard NM-64 design, PSNM should be useful for as long as a decade with minimal maintenance. The information is also important regarding space weather at Earth, which affects human activities such as communications satellite systems and other electrical systems. For example, the recent shutdown of Thai Com 5 in April, 2011 was likely a space weather effect associated with the arrival of a CME the preceding day. Neutron monitor data could in principle help provide advance warning of such space weather effects at Earth (Ruffolo, 1999; Leerungrat, 2003).

PSNM was established in 2007 by a collaboration involving three universities in Thailand: Mahidol University, Chulalongkorn University, and Ubon Ratchathani University. The measurement equipment was largely donated by Shinshu University, Japan and much technical knowledge and support has been provided by the University of Delaware, U.S.A. Figure 3.1 below shows the logo of the PSNM station, showing an atmospheric cascade above the station.



Figure 3.1 The PSNM station logo

3.2 Installation

The building was designed with a roof in an “A” shape, like other buildings in the Royal Thai Air Force base at which it is located (Figure 3.2). The floor, roughly sized $10 \times 10 \text{ m}^2$, was made of solid concrete to support a great weight, because the neutron monitor components weigh about 40 tons. There are triple doors to help prevent rain and humidity from entering the building. The roof is made of zinc and the walls have two layers of rock-wood with foam and heat reflector in the middle. The setup of the PSNM measurement system was started by installing polyethylene reflector and lead rings to surround each of the 18 proportional counter tubes for the NM-64. Three bare counters were also installed. After that, the electronics system of each tube was connected to a master electronics rack, which was in turn connected to the computer, with Visual Basic software to record count rates automatically. Since Doi Inthanon is far from the locations of our campuses and it is difficult to travel there, we installed a satellite-dish internet connection to send data to the main computers of our laboratories.

We also installed a GPS antenna to indicate the exact position and time to compare with international standards. A very precise pressure sensor has been installed to provide pressure data with which to calculate the pressure corrected neutron count rate. To control the humidity within the station, we have installed a dehumidifier that can absorb water vapor from the room.

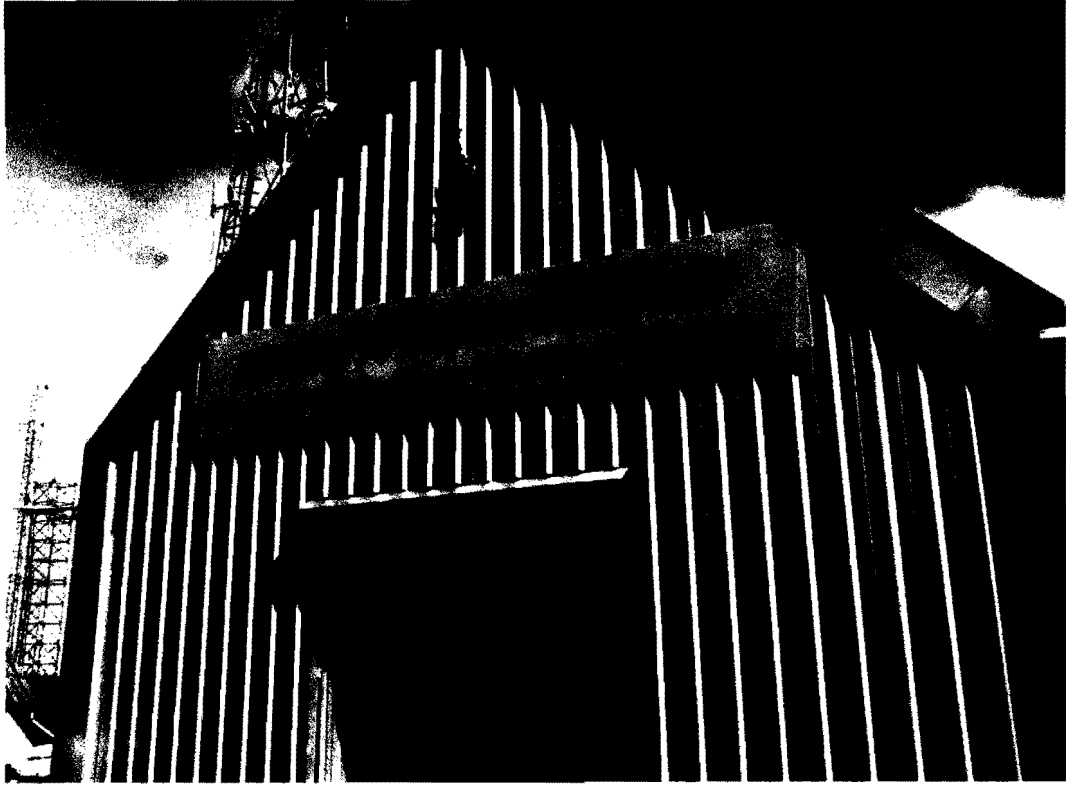
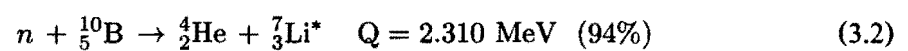
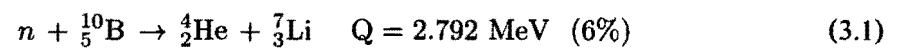


Figure 3.2 The Princess Sirindhorn Neutron Monitor building.

We also installed a weather station in order study possible weather effects on the neutron monitor measurements.

3.3 Data acquisition

There are 18 tubes in the neutron monitor and 3 bare counters inside the station as seen in Figure 3.3. These are proportional counter tube (see Figure 3.4) filled with $^{10}\text{B F}_3$. After a secondary atmospheric cosmic rays, a slow neutron can be captured by a ^{10}B nucleus and induces the reactions:



The reactions leave a lithium ion, either in the ground state (6%) or excited state (94%), and

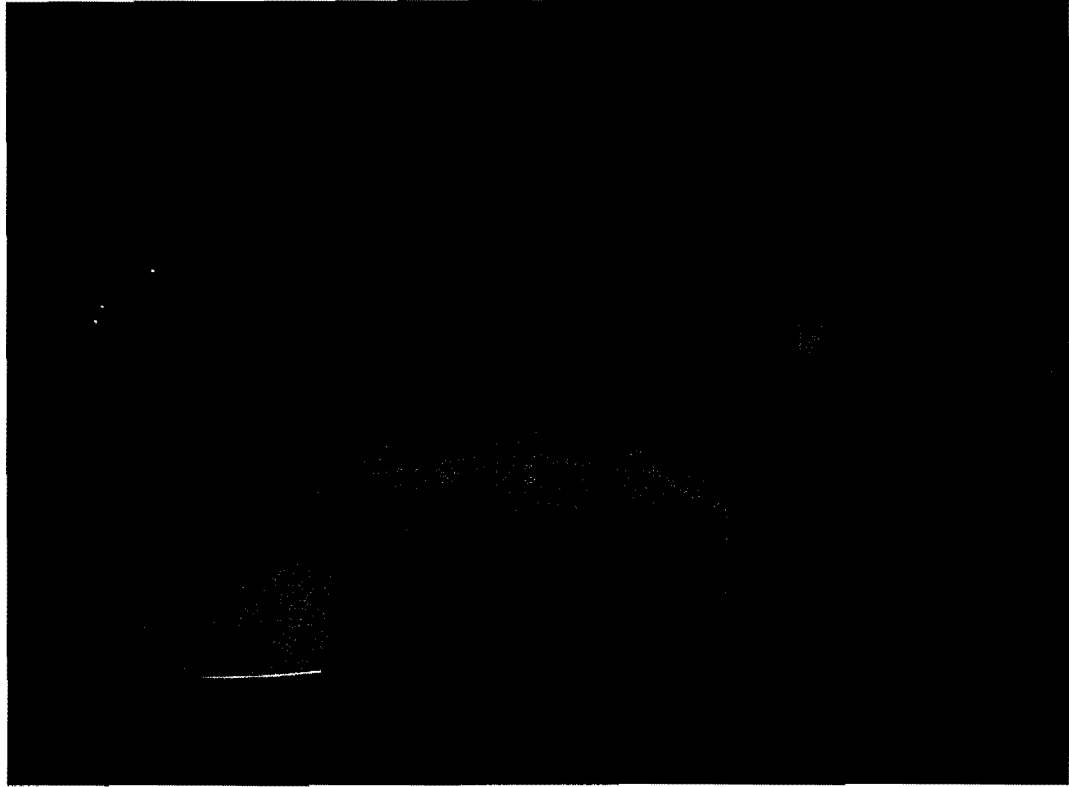


Figure 3.3 The 18 counter tubes of the neutron monitor and 3 bare counters inside the PSNM station. Note also the dehumidifier at the front. The computer and master electronics are on the table.

an alpha particle. The lithium and alpha cause ionization in the counter, which gives an output signal by using an electric field to separate and count the electrons. The signal is converted to hexadecimal by the electronics and sent to a computer program in Visual Basic that records the data automatically (Figure 3.5). In Figure 3.5, we see that the NM tubes count with a rate ~ 34 Hz/tube, but the bare count rate is about 6 times lower than the NM count rate because the bares do not have the lead producer that can produce more neutrons and amplify the signal.

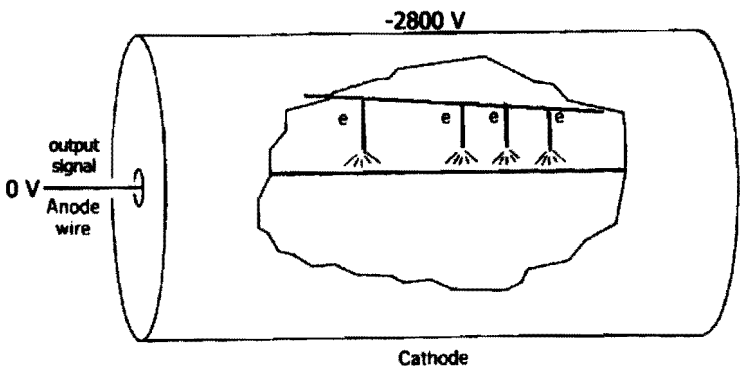


Figure 3.4 In the proportional counter, ion pairs are created and separated by an electric field.
This drawing has been modified from Krane (1988)

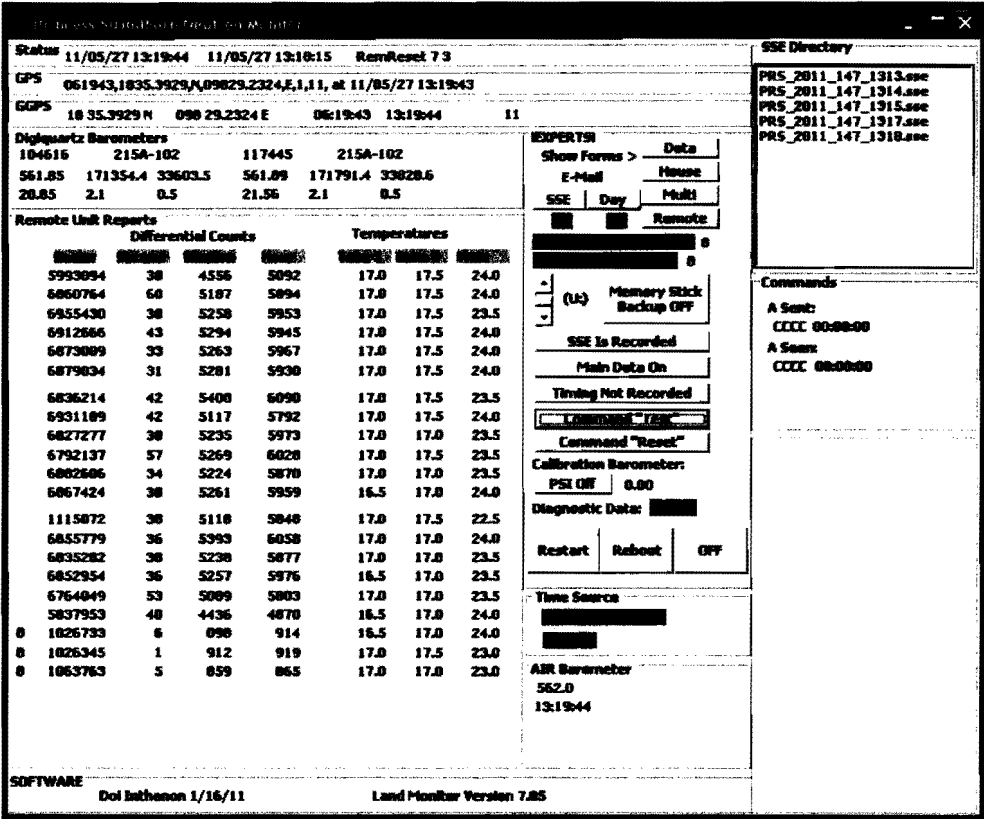


Figure 3.5 The main window of the Visual Basic program that records the neutron monitor data.
Note that near the center there are 18 rows corresponding to the 18 NM counter tubes and 3 rows corresponding to the 3 bare counters. The bare counters have a much lower count rate.

CHAPTER 4

NUMERICAL METHODS

When higher energy cosmic rays hit the upper atmosphere and generate a cascade reaction known as Extensive Air Shower. In order to understand the cosmic rays air shower. We using a Monte Carlo simulation of particle transport indicate the effect of the air mass to the secondary neutron above the PSNM . In this chapter we have explained the principle of the Monte Carlo method and Fluka program.

4.1 Monte Carlo methods

Monte Carlo methods (or Monte Carlo experiments) are a class of computational algorithms that rely on repeated random sampling to compute their results. Monte Carlo methods are often used in computer simulations of physical and mathematical systems. Monte Carlo named by Nicholas Metropolis and Stanislaw Ulam, while they were working on nuclear weapon projects (Manhattan Project) in the Los Alamos National Laboratory. It was named after the Monte Carlo Casino, a famous casino where Ulam's uncle often gambled away his money (Metropolis, 1987). Monte Carlo methods vary, but tend to follow a particular pattern:

- (1) Define a domain of possible inputs.
- (2) Generate inputs randomly from a probability distribution over the domain.
- (3) Perform a deterministic computation on the inputs.
- (4) Aggregate the results.

A Monte Carlo simulation of particle transport can be constructed if the probability distribution is known for each process. In this method, particle transport is simulated as a sequence of flights along a trajectory where each flight length is a random variable depending on the process cross-section of the material. As with a theoretical calculation, the Monte Carlo method does not necessarily rely on observational data and requires very accurate input data of fundamental transport quantities. The major difference is that the Monte Carlo attempts to simulate all the significant physical mechanisms in the expected time sequence producing a history of particle tracks. In general the Monte Carlo is used to generate a population of cascades and the history of each cascade in the form of particle tracks is recorded. The recorded data can then be used to

determine spectra fluences scored for different particle species. In this work the propagation of primary particles through the Earth's atmosphere was also simulated with FLUKA program. and then the results are weighted by the detection efficiency of a neutron monitor to determine the counting rate.

4.2 What is FLUKA

FLUKA is a program for calculations of particle transport and interactions with matter base on Monte Carlo simulations. The name FLUKA is short for the German words "FLUktuierende KAskade" which means "Fluctuating Cascade." There are many applications for physics, including particle detector and cosmic ray studies.

The highest priority in the design and development of Fluka has always been the implementation and improvement of sound and modern physical models. Microscopic models are adopted whenever possible, consistency among all the reaction steps and/or reaction types is ensured, conservation laws are enforced at each step, results are checked against experimental data at single interaction level. As a result, final predictions are obtained with a minimal set of free parameters fixed for all energy/target/projectile combinations. Therefore results in complex cases, as well as properties and scaling laws, arise naturally from the underlying physical models, predictivity is provided where no experimental data are directly available, and correlations within interactions and among shower components are preserved.

Fluka can simulate with high accuracy the interaction and propagation in matter of about 60 different particles, including photons and electrons from 1 keV to thousands of TeV, neutrinos, muons of any energy, hadrons of energies up to 20 TeV (up to 10 PeV by linking Fluka with the Dpmjet code) and all the corresponding antiparticles, neutrons down to thermal energies and heavy ions. The program can also transport polarised photons (e.g., synchrotron radiation) and optical photons. Time evolution and tracking of emitted radiation from unstable residual nuclei can be performed on line.

Fluka can handle even very complex geometries, using an improved version of the well-known Combinatorial Geometry (CG) package. The Fluka CG has been designed to track correctly also charged particles (even in the presence of magnetic or electric fields). Various visualisation and debugging tools are also available.

For most applications, no programming is required from the user. However, a number of user interface routines (in Fortran 77) are available for users with special requirements.

The Fluka physical models are described in several journal and conference papers; on the technical side the stress has been put on four apparently conflicting requirements, namely efficiency, accuracy, consistency and flexibility.

Efficiency has been achieved by having a frequent recourse to table look-up sampling and a systematic use of double precision has had a great impact on overall accuracy: both qualities have benefited from a careful choice of the algorithms adopted. To attain a reasonable flexibility while minimising the need for user-written code, the program has been provided with a large number of options available to the user, and has been completely restructured introducing dynamical dimensioning.

Another feature of Fluka, probably not found in any other Monte Carlo program, is its double capability to be used in a biased mode as well as a fully analogue mode. That means that while it can be used to predict fluctuations, signal coincidences and other correlated events, a wide choice of statistical techniques are also available to investigate punchthrough or other rare events in connection with attenuations by many orders of magnitude.

4.3 FLUKA's physics, structure and capabilities

Here we only give a very short summary list of the capabilities and limitations of Fluka, since this is meant to be mainly a practical guide. More detailed descriptions of the physical models, algorithms and techniques will be found in cited references. (Ferrari, et al., 2005)

4.3.1 Physics

4.3.1.1 Hadron inelastic nuclear interactions

The Fluka hadron-nucleon interaction models are based on resonance production and decay below a few GeV, and on the Dual Parton model above. Two models are used also in hadron-nucleus interactions. At momenta below 3-5 GeV/c the PEANUT package includes a very detailed Generalised Intra-Nuclear Cascade (GINC) and a preequilibrium stage, while at high energies the Gribov-Glauber multiple collision mechanism is included in a less refined GINC. Both modules are followed by equilibrium processes: evaporation, fission, Fermi break-up, gamma deexcitation. Fluka can also simulate photonuclear interactions (described by Vector Meson Dominance, Delta Resonance, Quasi-Deuteron and Giant Dipole Resonance).

4.3.1.2 Elastic Scattering

- 1) Parameterised nucleon-nucleon cross sections.
- 2) Tabulated nucleon-nucleus cross sections.

3) Tabulated phase shift data for pion-proton and phase-shift analysis for kaon-proton scattering.

4) Detailed kinematics of elastic scattering on hydrogen nuclei and transport of proton recoils.

4.3.1.3 Nucleus-Nucleus interactions

Nuclear interactions generated by ions are treated through interfaces to external event generators.

1) Above 5 GeV per nucleon: Dpmjet-II or Dpmjet-III with special initialisation procedure.

2) Between 0.1 and 5 GeV per nucleon: modified RQMD (Relativistic Quantum Molecular Dynamics).

3) Below 0.1 GeV per nucleon: BME (Boltzmann Master Equation).

4.3.1.4 Low-energy neutrons

For neutrons with energy lower than 20 MeV, Fluka uses its own neutron cross section library (P5 Legendre angular expansion, 260 neutron energy groups) containing more than 250 different materials, selected for their interest in physics, dosimetry and accelerator engineering and derived from the most recently evaluated data:

1) multigroup P5 cross sections with 260 groups.

2) Gamma-ray generation and different temperatures available.

3) Doppler broadening for temperatures above 0 K.

4) Standard multigroup transport with photon and fission neutron generation.

5) Detailed kinematics of elastic scattering on hydrogen nuclei.

6) Transport of proton recoils and protons from N(n,p) reaction.

7) Capture photons generated according to the multigroup treatment, but transported with the more accurate Emf package which performs continuous transport in energy and allows for secondary electron generation.

4.3.1.5 Photons

1) Pair production with actual angular distribution of electrons and positrons.

2) Landau-Pomeranchuk-Migdal pair production suppression effect.

3) Compton effect with Doppler broadening using a fit of the Compton

profiles and account for atomic bonds through use of inelastic Hartree-Fock form factors.

4) Photoelectric effect with actual photoelectron angular distribution according to the fully relativistic theory of Sauter. Interactions sampled separately for each component element and for each edge. The edge fine structure is taken into account.

Parameterisations/tabulations for photoelectric cross sections including all known edges up to $Z = 100$ and down to a few eV. Optional emission of fluorescence photons and approximate treatment of Auger electrons for all K and most L lines.

5) Rayleigh scattering.

6) Photon polarisation taken into account for Compton, Rayleigh and Photoelectric effects.

7) Photohadron production.

8) Vector Meson Dominance Model modified and improved using PEANUT below 770 MeV.

9) Quasideuteron interactions.

10) Giant Dipole Resonance.

4.3.2 Geometry

A part of the code where efficiency, accuracy, consistency and flexibility have combined giving very effective results is the Fluka geometry. Derived from the Combinatorial Geometry package, it has been entirely rewritten. A completely new, fast tracking strategy has been developed, with special attention to charged particle transport, especially in magnetic fields. New bodies have been introduced, resulting in increased rounding accuracy, speed and even easier input preparation.

4.3.2.1 Combinatorial Geometry (CG) with additional bodies (infinite circular and elliptical cylinder parallel to X,Y,Z axis, generic plane, planes perpendicular to the axes, generic quadrics).

4.3.2.2 Possibility to use body and region names instead of numbers.

4.3.2.3 Possibility of using body combinations inside nested parentheses.

4.3.2.4 Geometry directives for body expansions and roto-translation transformations.

4.3.2.5 Distance to nearest boundary taken into account for improved performance.

4.3.2.6 Accurate treatment of boundary crossing with multiple scattering and magnetic or electric fields.

4.3.2.7 The maximum number of regions (without recompiling the code) is 10000.

4.3.2.8 The tracking strategy has been substantially changed with respect to the original CG package. Speed has been improved and interplay with charged particle transport (multiple scattering, magnetic and electric field transport) has been properly set.

4.3.2.9 A limited repetition capability (lattice capability) is available. This allows to avoid describing repetitive structures in all details. Only one single module has to be described and then can be repeated as many times as needed. This repetition does not occur at input stage but is hard-wired into the geometry package, namely repeated regions are not set up in memory, but the given symmetry is exploited at tracking time using the minimum amount of bodies/regions required. This allows in principle to describe geometries with even tens of thousands regions (e.g., spaghetti calorimeters) with a reasonable number of region and body definitions.

4.3.2.10 Voxel geometry is available on option, completely integrated into CG.

4.3.3 Transport

4.3.3.1 Condensed history tracking for charged particles, with single scattering option.

4.3.3.2 Time-cutoff.

4.3.3.3 Legendre angular expansion for low-energy neutron scattering.

4.3.3.4 Transport of charged particles in magnetic and electric fields.

4.3.4 Biasing

4.3.4.1 Leading particle biasing for electrons and photons: region dependent, below user-defined energy threshold and for selected physical effects.

4.3.4.2 Russian Roulette and splitting at boundary crossing based on region relative importance.

4.3.4.3 Region-dependent multiplicity reduction in high energy nuclear interactions.

4.3.4.4 Region-dependent biased downscattering and non-analogue absorption of low-energy neutrons.

4.3.4.5 Biased decay length for increased daughter production.

4.3.4.6 Biased inelastic nuclear interaction length.

4.3.4.7 Biased interaction lengths for electron and photon electromagnetic

interactions.

4.3.4.8 Biased angular distribution of decay secondary particles.

4.3.4.9 Region-dependent weight window in three energy ranges (and energy group dependent for low-energy neutrons).

4.3.4.10 Bias setting according to a user-defined logics.

4.3.4.11 User-defined neutrino direction biasing.

4.3.4.12 User-defined step by step importance biasing.

4.3.5 Scoring

4.3.5.1 Star density by producing particle and region.

4.3.5.2 Energy density by region, total or from electrons/photons only.

4.3.5.3 Star, energy and momentum transfer density and specific activity in a geometry-independent binning structure (Cartesian or cylindrical), averaged over the run or event by event.

4.3.5.4 Energy deposition weighted by a quenching factor (Birks law).

4.3.5.5 Step size independent of bin size.

4.3.5.6 Time window.

4.3.5.7 Coincidences and anti-coincidences.

4.3.5.8 Fluence and current scoring as a function of energy and angle, via boundary crossing, collision and track-length estimators coincident with regions or region boundaries.

4.3.5.9 Dose Equivalent via boundary-crossing, collision and track-length estimators coincident with regions or region boundaries, convoluted with conversion coefficients or obtained multiplying doses by a LET dependent quality factor.

4.3.5.10 Track-length fluence or Dose Equivalent in a binning structure (Cartesian or cylindrical) independent of geometry.

4.3.5.11 Particle yield from a target or differential cross section with respect to several different kinematic variables.

4.3.5.12 Residual nuclei.

4.3.5.13 Fission density.

4.3.5.14 Momentum transfer density.

4.3.5.15 Neutron balance.

4.3.5.16 No limit to the number of detectors and binnings within the total memory available (but a maximum number must be fixed at compilation time).

4.3.5.17 Energy deposition can be scored on option disregarding the particle weights (useful for studying computer performance, etc.).

4.3.5.18 All quantities from radioactive decay of residual nuclei can be scored according to user-defined irradiation and cooling time profiles.

4.3.6 Code structure, technical aspects

4.3.6.1 The whole program, including the numerical constants, is coded in double precision (at least the versions for 32-bit word machines). The only exceptions are the low-energy neutron cross sections, which are stored in single precision to save space.

4.3.6.2 Consistent use of the latest recommended set of physical constant values.

4.3.6.3 Dynamical memory allocation is implemented as far as possible.

4.3.6.4 Extensive use of INCLUDE and of constant parameterisation.

4.3.6.5 64-bit random number generator.

4.3.7 Applications

While Fluka of the '86s-87s was essentially a specialised program to calculate shielding of high energy proton accelerators, the present version can be regarded as a general purpose tool for an extended range of applications. In addition to traditional target design and shielding, applications are now spanning from calorimetry to prediction of activation, radiation damage, isotope transmutation, dosimetry and detector studies. Prediction of radiation damage has always been a traditional field of application of Fluka, restricted however in earlier versions to hadron damage to accelerator components. The new capability to deal with the low-energy neutron component of the cascade has extended the field of interest to include electronics and other sensitive detector parts. In addition, radiation damage calculations and shielding design are not limited to proton accelerators any longer, but include electron accelerators of any energy, photon factories, and any kind of radiation source, be it artificial or natural.

The present version of Fluka has been used successfully in such diverse domains as background studies for underground detectors, cosmic ray physics, shielding of synchrotron radiation hutches, calculation of dose received by aircraft crews, evaluation of organ dose in a phantom due to external radiation, detector design for radiation protection as well as for high energy physics, electron, proton and heavy ion radiotherapy, nuclear transmutation, neutrino physics, shielding of free-electron lasers, calculation of tritium production at electron accelerators, energy amplifiers, maze design for medical accelerators, etc.

CHAPTER 5

MODELING OF ATMOSPHERIC CASCADES

In order to simulate secondary cosmic ray we use the FLUKA program, FLUKA is maintained and developed under INFN (Italian National Institute for Nuclear Physics) and CERN (European Organization for Nuclear Research agreement) which own copyrights for 1989 - 2008 (Ferrari, et al., 2005; Battistoni, 2007) . The input file (*.inp) is created by the user and there are some user interface routines, based on Fortran 77, for special requirements. FLUKA input files are general “TEXT” files which consist of FLUKA commands on one line or more, each called a “CARD”, and variables or numbers. We can create our detector system with any shape and any material composition including definitions of geometry, materials, and particle sources. The program creates a random number sequence to start the simulation. There are many definitions in the output files, for example, the type of secondary particle, energy, type of interaction, simulated position vector, etc., that let us know what happened during and after the simulated interactions of the requested particles. In this thesis, we model the Earth’s atmosphere and examine the numbers of neutrons that are produced in the atmosphere from primary protons. The main processes of modeling are described in following sections.

5.1 Model Standard atmosphere

In the U.S. Standard Atmosphere (NOAA, 1976), the atmosphere is separated into seven layers (Table 5.1) according to the altitude, up to 85 km from sea level. Within each layer, the temperature is taken to change with a constant temperature lapse rate (L). The pressure and density of air decrease with increasing altitude. Table 5.2 shows the atmospheric composition according to the U.S. Standard Atmosphere (1976), in terms of the percent by volume and by weight for each compound or element. Table 5.2 refers to standard dry air. If we need to include the abundance of water vapor, we will include H_2O in an amount that varies linearly from 0.06% by weight at sea-level to 0.01% by weight at 2000 meters and is set to a constant value of 0.01 % by weight above 2000 m (Clem, 2003).

Table 5.1 The U.S. Standard Atmosphere altitude profile

Range	Height Above	Mass	Static Pressure	Temperature	Standard
<i>b</i>	Sea Level (<i>h</i>)	Density (ρ)	(<i>P</i>)	Lapse Rate (<i>L</i>)	Temperature (<i>T</i>)
	[m]	[kg/m ²]	[pascals]		[K]
0	0	1.225	101325.00000	-0.0065	288.15
1	11000	0.36391	22632.10000	0.0	216.65
2	20000	0.08803	5474.89000	0.001	216.65
3	32000	0.01322	868.01900	0.0028	228.65
4	47000	0.00143	110.90600	0.0	270.65
5	51000	0.00086	66.93890	-0.0028	270.65
6	71000	0.000064	3.95642	-0.002	214.65

Table 5.2 The U.S. Standard Atmosphere composition

Gas	Form	% by Volume	% by Weight	Molecular Weight
Nitrogen	N ₂	78.08	75.47	28.01
Oxygen	O ₂	20.95	23.2	32.00
Argon	Ar	0.93	1.28	39.95
Carbon Dioxide	CO ₂	0.038	0.059	44.01
Neon	Ne	0.0018	0.0012	20.18
Helium	He	0.0005	0.00007	4.00
Krypton	Kr	0.0001	0.0003	83.80
Hydrogen	H ₂	0.00005	Negligible	2.02
Xenon	Xe	8.70E-06	0.00004	131.30

5.1.1 Pressure equations

For more specific values, the pressure is specified versus the altitude from sea level by

$$P = P_b \cdot \left[\frac{T_b}{T_b + L_b(h - h_b)} \right]^{\frac{g \cdot M}{R \cdot L_b}} \quad \text{if } L_b \neq 0,$$

(5.1)

$$P = P_b \cdot \exp \left[\frac{-g \cdot M \cdot (h - h_b)}{R \cdot T_b} \right] \quad \text{if } L_b = 0, \quad (5.2)$$

Where P_b = Static pressure (pascals), T_b = Standard temperature (K), L_b = Standard temperature lapse rate (K/m), h = Height above sea level (m), h_b = Height at bottom of range b (m), R = Universal gas constant for air (8.31432 N·m/(mol·K)), g = Standard gravitational acceleration (9.80665 m/s²), M = Molar mass of Earth's air (0.0289644 kg/mol). The range b refers to the index of the altitude layer in Table 5.1. The above equations are derived in Appendix B.

5.1.2 Density equations

Similarly, the air density can also be specified versus the altitude from sea level by

$$\rho_b \equiv \frac{1}{h_{b+1} - h_b} \int_{h_b}^{h_{b+1}} \rho(z) \cdot dz \quad (5.3)$$

$$\rho_b = -\frac{P_{b+1} - P_b}{g \cdot (h_{b+1} - h_b)} \quad (5.4)$$

The above equations are derived in Appendix B.

5.2 Geometry and materials

This section defines the geometry of atmosphere, “constructed” in the simulation with appropriate materials. FLUKA simulations generally also create VACUUM and BLACK HOLE layers for interactions of particles outside the system in VACUUM and stop all interactions when entering the BLACK HOLE. Our model assumes that the air mass can be neglected above 51 km of altitude; this accounts for only 0.04% of the atmosphere's mass. Up to this altitude, we can ignore the curvature of the Earth because this is less than 1% of Earth's radius (6378 km).

We divide the atmosphere into 100 layers within a rectangular box (Figure 5.1).

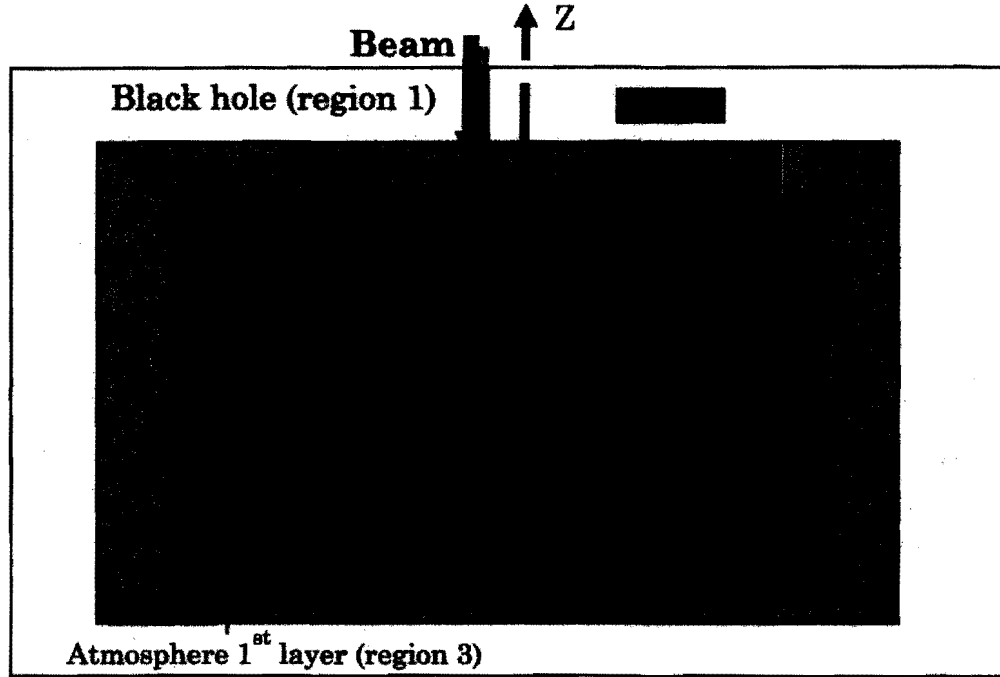


Figure 5.1 The atmospheric model including 100 layers of the atmosphere from sea level and two special regions, VACUUM and BLACK HOLE, for the FLUKA simulation.

We set 20 km of horizontal length for each side. The properties of each layer were determined as follows:

The layers were defined so that each layer has approximately the same air mass (see Table 5.3). Within a range b , we use

$$\Delta P_b = \frac{P_{b+1} - P_b}{i_{2,b} - i_{1,b} + 1} \quad (5.5)$$

$$P_i = P_b + (i - i_{1,b}) \cdot \Delta P_b \quad (5.6)$$

The altitude for each layer can be calculated in terms of the pressure:

$$h_i(P_i) = h_{i-1} + \frac{T_b}{L_b} \cdot \left[\left(\frac{P_i}{P_{i-1}} \right)^{-\frac{R \cdot L_b}{g \cdot M}} - 1 \right] \quad \text{if } L_b \neq 0, \quad (5.7)$$

$$h_i(P_i) = h_{i-1} - \frac{R \cdot T_b}{g \cdot M} \cdot \ln \left(\frac{P_i}{P_{i-1}} \right) \quad \text{if } L_b = 0 \quad (5.8)$$

The density equation was derived for hydrostatic equilibrium in terms of pressure and altitude:

$$\rho_i \equiv \frac{1}{h_{i+1} - h_i} \int_{h_i}^{h_{i+1}} \rho(z) \cdot dz \quad (5.9)$$

$$\rho_i = - \frac{P_{i+1} - P_i}{g \cdot (h_{i+1} - h_i)} \quad (5.10)$$

Within each range b , the temperature was assumed to be a linear function with a constant slope with altitude (i.e., constant temperature lapse rate), according to Table 5.3. We also included the chemical composition of air, using a constant molecular composition above 2000 meters with 75.512% N₂, 23.19% O₂, 1.282% Ar and 0.016% CO₂ and included H₂ in an amount that varies linearly from 0.06% by mass at sea-level to 0.01% by weight at 2000 meters and is set to a constant value of 0.01 % by weight above 2000 m (Clem et al., 2003). Note that we ignore the molecules with < 0.05 % by weight in Table 5.2 and renormalize the remaining components' percentages by weight so they sum to 100. Because FLUKA needs the atomic composition for the simulation format, we calculated the atomic composition, using the molecular weights, for each layer. From the sea level to 2000 m the atomic composition changed, and it was constant above 2000 m.

We created the ground (mountain) region at 2565 m of altitude with granite (most of the rock at Doi Inthanon) (see Table 5.4) to model the particle propagation through and interactions in this region. We also calculated the atomic composition of the granite for FLUKA input as shown in Table 5.5.

5.3 Source particles

We create initial particles as a set of 300 protons moving vertically downward from the top of the atmosphere, in the VACUUM region, over an area of 1 cm². Their kinetic energy was set as follows: 10, 11, 12, 13, 14, 15, 16, 17, 18, 19, 20, 21, 22, 25, 30, and 100 GeV.

Table 5.3. Properties of our layers for Monte Carlo modeling, based on the U.S. Standard Atmosphere

Range	Layer number	Height Above	Mass	Static Pressure	Temperature	Standard
<i>b</i>	(<i>i</i>)	Sea Level (<i>h</i>)	Density (ρ)	(<i>P</i>)	Lapse Rate (<i>L</i>)	Temperature (<i>T</i>)
		[m]	[kg/m ²]	[pascals]		[K]
0	1 - 77	0 - 11000	1.225	101325.0	-0.0065	288.15
1	78 - 94	11000 - 20000	0.36391	22632.1	0.0	216.65
2	95 - 98	20000 - 32000	0.08803	5474.89	0.001	216.65
3	99	32000 - 47000	0.01322	868.019	0.0028	228.65
4	100	47000 - 51000	0.00143	110.906	0.0	270.65

Table 5.4 The molecular composition of granite, used in the the material composition for the mountain

Molecule	% by Weight
SiO ₂	72.04%
Al ₂ O ₃	14.42%
K ₂ O	4.12%
Na ₂ O	3.69%
CaO	1.82%
FeO	1.68%
Fe ₂ O ₃	1.22%
MgO	0.71%
TiO ₂	0.30%
P ₂ O ₅	0.12%
MnO	0.05%

Table 5.5 Atomic composition of the granite at 2565 m for the mountain

Atom	% by Weight	Atomic Weight
O	48.55	16.00
Si	33.68	28.09
Al	7.63	26.98
K	3.42	39.10
Na	2.74	22.98
Ca	1.30	40.08
Fe	2.16	55.84
Mg	0.43	24.30
Ti	0.18	47.87
P	0.05	30.98
Mn	0.04	54.94

5.4 Readout setting

FLUKA normally prints out an output file containing all the interaction information of the simulation produce. We have modified the user routine file, called MGDRAW, to produce a special printout file containing only the information of interest. This includes the type of particle, type of interaction, initial particle index, total energy, XYZ-position and velocity vector as described below. These also specify the particles at 2565 meters of altitude.

JTRACK = particle type
 NCASE = number of primaries treated so far (including the current one)
 ICODE indicates the type of point event giving rise to energy deposition,
 ICODE = 1X: call from subroutine KASKAD (hadronic part of FLUKA);
 = 19: boundary crossing
 ICODE = 2X: call from subroutine EMFSCO (electromagnetic part of FLUKA);
 = 29: boundary crossing
 ICODE = 3X: call from subroutine KASNEU (low-energy neutron part of FLUKA);
 = 39: boundary crossing
 XSCO, YSCO, ZSCO = coordinates of the energy deposition point
 ETRACK = total energy of the particle (rest + kinetic)
 Cx, y, ztrck = direction cosines of the current particle
 MREG = region from which the particle is exiting
 NEWREG = region the particle is entering
 WTRACK = particle weight (statistical meaning)

5.5 Programming

We create the FLUKA input files by writing a C program that helps us to generate input files matching the specific format of FLUKA. A FLUKA input file is an ASCII “standard input” file with extension .inp, containing a variable number of commands, called “CARDS”, in one or more lines. The following sections briefly define input cards related to the previous sections. More command options and definitions are described in the manual (Ferrari, 2005).

5.5.1 Geometry definition

```
*...+....1....+....2....+....3....+....4....+....5....+....6....+....7....+....8
GEOBEGIN
0 -10 A rectangular parallelepiped inside vacuum
RPP Rpp001 -5.000e+08 5.000e+08 -5.000e+08
5.000e+08 -5.000e+08 5.000e+08
RPP Rpp002 -2.500e+08 2.500e+08 -2.500e+08
2.500e+08 -2.500e+08 2.500e+08
* set ground at 0.0 m
RPP Rpp003 -2.000e+06 2.000e+06 -2.000e+06
2.000e+06 0.000e+00 8.542e+03
RPP Rpp004 -2.000e+06 2.000e+06 -2.000e+06
2.000e+06 0.000e+00 1.716e+04
END
*...+....1....+....2....+....3....+....4....+....5....+....6....+....7....+....8
* black hole
Blackhole 2 +Rpp001 -Rpp002
* vacuum around
Vacarund 2 +Rpp002 -Rpp102
* atmospheric layers
Layer001 2 +Rpp003
Layer002 2 +Rpp004 -Rpp003
Layer003 2 +Rpp005 -Rpp004
END
GEOEND
*...+....1....+....2....+....3....+....4....+....5....+....6....+....7....+....8
```

The definitions between GEOBEGIN and GEOEND start with RPP for a rectangular parallelepiped. The second column is the name of the body with a reference number and next are geometrical parameters for each body over two lines. A line with “*” is a definition or column heading. The second part after the first END starts with the name of the region. All of them connect with two other regions in the second column. The positive or negative numbers show the inclusion or exclusion of a body for each region. For example, region “Layer003” is formed by “Rpp005” minus “Rpp004”.

5.5.2 Material definition and assignment

*...+...1...+...2...+...3...+...4...+...5...+...6...+...7...+...8							
*CARD	WHAT-1	WHAT-2	WHAT-3	WHAT-4	WHAT-5	WHAT-6	SDUM
*MATERIAL	Z	A	Density	FLUKA#	ionize	isotope	ElemLAY#
*...+...1...+...2...+...3...+...4...+...5...+...6...+...7...+...8							
MATERIAL	8.0	15.9994	1.429e-03	8			OXYGEN
LOW-MAT	8	8.0	16.0	296.0			OXYGEN
MATERIAL	12.0	24.305	1.738	9			MAGNESIU
LOW-MAT	9	12.0	-2.0	296.0			MAGNESIU
MATERIAL	13.0	26.982	2.70	10			ALUMINUM
LOW-MAT	10	13.0	27.0	296.0			ALUMINUM
MATERIAL	26.0	55.847	7.877	11			IRON
LOW-MAT	11	26.0	-2.0	296.0			IRON
MATERIAL	14.0	28.086	2.33	14			SILICON
LOW-MAT	14	14.0	-2.0	296.0			SILICON
MATERIAL	11.0	22.989	0.971	19			SODIUM
LOW-MAT	19	11.0	23.0	296.0			SODIUM
MATERIAL	20.0	40.08	1.55	21			CALCIUM
LOW-MAT	21	20.0	-2.0	296.0			CALCIUM
*...+...1...+...2...+...3...+...4...+...5...+...6...+...7...+...8							
MATERIAL	19.0	39.098	0.862	26			POTASSIU
LOW-MAT	26	19.0	-2.0	296.0			POTASSIU
*...+...1...+...2...+...3...+...4...+...5...+...6...+...7...+...8							
MATERIAL	0.0	0.0	2.75	27			GNEISS
COMPOUND	-48.55	OXYGEN	-33.68	SILICON	-7.63	ALUMINUM	GNEISS
COMPOUND	-3.42	POTASSIU	-2.74	SODIUM	-1.13	CALCIUM	GNEISS
COMPOUND	-2.16	IRON	-0.43	MAGNESIU			GNEISS
MAT-PROP	0.9769	31	296	OXYGEN	GNEISS	1.0	LOWNTEMP
*...+...1...+...2...+...3...+...4...+...5...+...6...+...7...+...8							
MATERIAL	6	12.01070	2.0000000	28	0.0	0.0	CLAY001
LOW-MAT	28	6	-2	296			CARBON
MATERIAL	7	14.00670	0.0011700	29	0.0	0.0	NLAY001
LOW-MAT	29	7	-2	296			NITROGEN
MATERIAL	8	15.99940	0.0013300	30	0.0	0.0	OLAY001
LOW-MAT	30	8	16	296			OXYGEN
MATERIAL	18	39.94800	0.0016600	31	0.0	0.0	ARLAY001
LOW-MAT	31	18	-2	296			ARGON
MATERIAL	1	1.00794	0.0000837	32	0.0	0.0	HLAY001


```
LOW-MAT      32      1      -2      296      HYDROGEN
MATERIAL      0      0  0.001220      33      LAY001
COMPOUND -75.297890  NLAY001-23.345525  OLAY001 -1.279590  ARLAY001  LAY001
COMPOUND  -0.016995  CLAY001 -0.060000  HLAY001      LAY001
MAT-PROP    0.972534      31      296      28      33      1.0LOWNTEMP
MAT-PROP    0.994957      0      -1      33
*...+....1....+....2....+....3....+....4....+....5....+....6....+....7....+....8
MATERIAL      6  12.01070  2.0000000      34      0.0      0.0  CLAY002
LOW-MAT      34      6      -2      296      CARBON
MATERIAL      7  14.00670  0.0011700      35      0.0      0.0  NLAY002
LOW-MAT      35      7      -2      296      NITROGEN
MATERIAL      8  15.99940  0.0013300      36      0.0      0.0  OLAY002
LOW-MAT      36      8      16      296      OXYGEN
MATERIAL     18  39.94800  0.0016600      37      0.0      0.0  ARLAY002
LOW-MAT      37     18      -2      296      ARGON
MATERIAL      1  1.00794  0.0000837      38      0.0      0.0  HLAY002
LOW-MAT      38      1      -2      296      HYDROGEN
MATERIAL      0      0  0.001210      39      LAY002
COMPOUND -75.299684  NLAY002-23.346081  OLAY002 -1.279621  ARLAY002  LAY002
COMPOUND  -0.016995  CLAY002 -0.057619  HLAY002      LAY002
MAT-PROP    0.970642      31      296      34      39      1.0LOWNTEMP
MAT-PROP    0.984871      0      -1      39
*...+....1....+....2....+....3....+....4....+....5....+....6....+....7....+....8
*ASSIGNMAT MATERIAL#      GEO#
ASSIGNMAT    LAY001  Layer001
ASSIGNMAT    LAY002  Layer002
ASSIGNMAT    LAY100  Layer100
ASSIGNMAT  BLCKHOLE  Blckhole
ASSIGNMAT    VACUUM  Vacarund
ASSIGNMAT    GNEISS  Layer101
```

The element materials are defined using the MATERIAL card, with WHAT-1 to WHAT-6 and SDUM (name of column). WHAT-1 defines the Z number of the element, WHAT-2 defines its mass number, WHAT-3 defines the material's density and WHAT-4 assigns its number. The SDUM option assigns the name of the material. The LOW-MAT card refers to a material in the FLUKA data base. The COMPOUND cards define a material composed of several elements, including the percentage by weight of atmospheric composition. The MAT-PROP card defines the temperature and density of the compound.

The ASSIGNMAT command is used to assign materials to each region, where WHAT-1 shows the name of the material and WHAT-2 defines the name of the region.

5.5.3 Beam definition and running FLUKA

```
BEAM          -100.0      0.0      0.0      1.0      1.0      1.0PROTON
BEAMPOS        0.0      0.0  5.12e+06                                NEGATIVE
*...+...1...+...2...+...3...+...4...+...5...+...6...+...7...+...8
USERDUMP       100      49      0.0      0.0
RANDOMIZE       1.0  4044900.
START          300.0
STOP
*...+...1...+...2...+...3...+...4...+...5...+...6...+...7...+...8
```

The BEAM card starts with the kinetic energy of the primary particle, whereas WHAT-4&5 define the beam width in the *x* and *y* directions in cm and the number 1.0 in WHAT-6 refers to the PROTON beam. Then BEAMPOS defines the initial position and direction of the beam. The USERDUMP command calls the user routine to activate MGDRAW. We can set any random seed in WHAT-2 of the RANDOMIZE card to start the random number sequence. The number of primary beam particles in the START card will have an impact on the running time and statistical error of the Monte Carlo simulation.

Finally, we run FLUKA for each kinetic energy of primary protons as shown in the diagram below (Figure 5.2). We will show and discuss the results in the next Chapter.

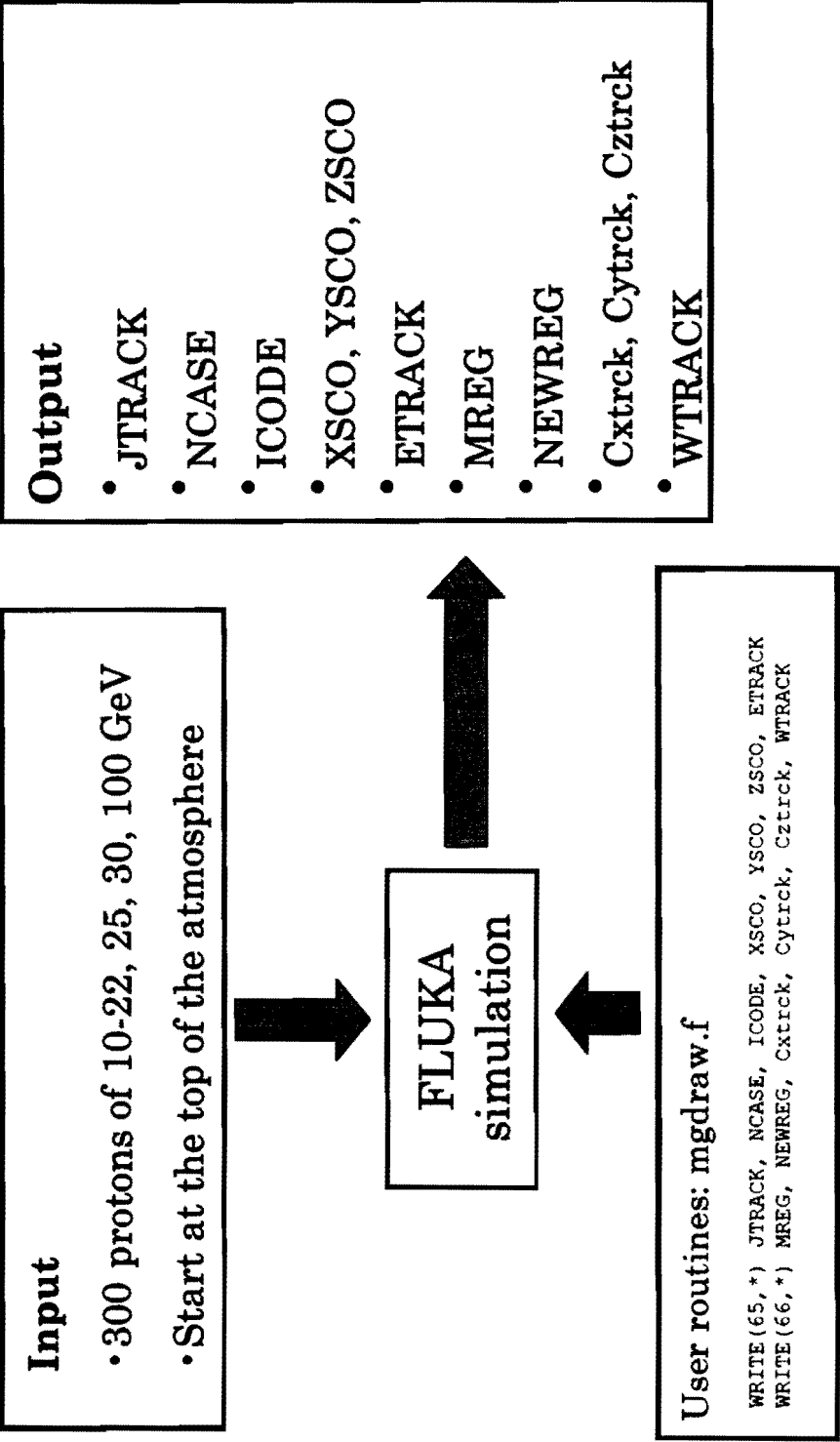


Figure 5.2. The diagram of the process of the FLUKA simulation for our atmospheric modeling.

CHAPTER 6
RESULTS AND DISCUSSION

6.1 Atmospheric cascade

The whole simulation was performed under Monte Carlo method by using FLUKA package in a 20 km x 20 km x 51 km volume above the PSNM. We used 9 different primary momentum at the same zenith angle which 300 cascades for each energy. The study also included the effects of the rock underneath the station into account. Figure 6.1 is the first simulation show the atmospheric cutoff energy near 1 GeV. This shows part of the atmospheric model and some of the secondary which most of them were absorbed before approaching the PSNM station (as indicated by a solid line in the picture).

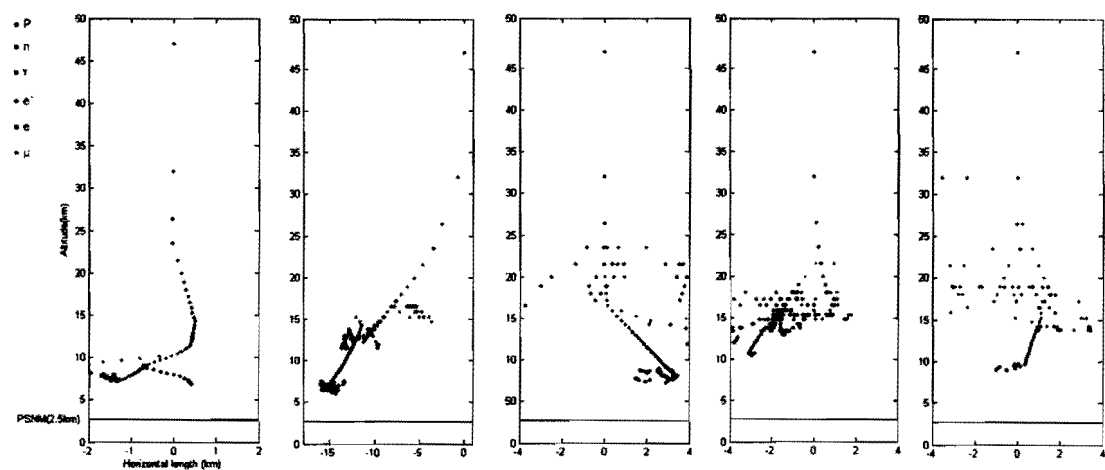


Figure 6.1 Shows the atmospheric cascade from 5 mono-energetic 1 GeV primary protons which is close to the atmospheric cutoff (1 GV)

For higher primary incident particles (protons) can produced more secondary particles as shown in Figure 6.2. In Figure 6.3 shows some part of the cascades from the simulation and the same situation as Figure 6.2 but we taking the effect of Doi Inthanon mountain beneath the station into account as shown in Figure 6.4.

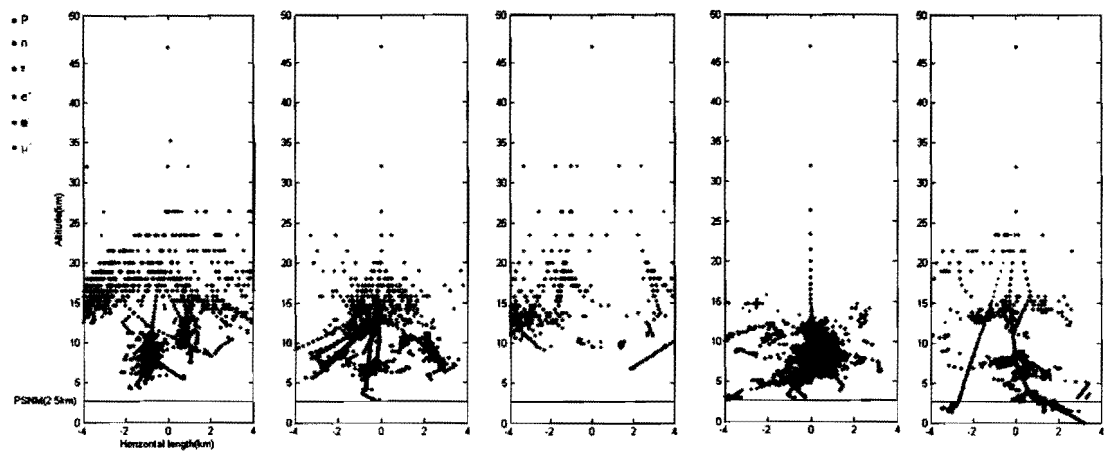


Figure 6.2 Atmospheric cascade form 5 primary protons which energy 10 GeV. Gamma rays are frequently created. There are a few neutrons reach the station.

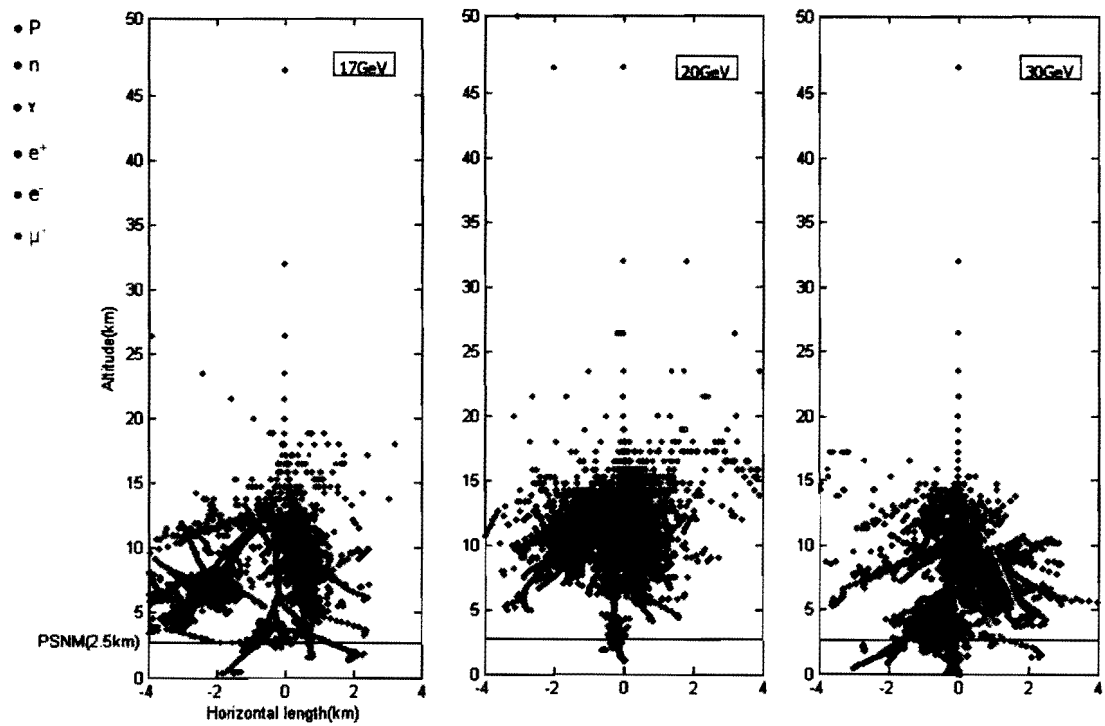


Figure 6.3 The cascades from 17, 20 and 30 GeV primary protons which the impact can produce many secondary neutrons and gamma rays

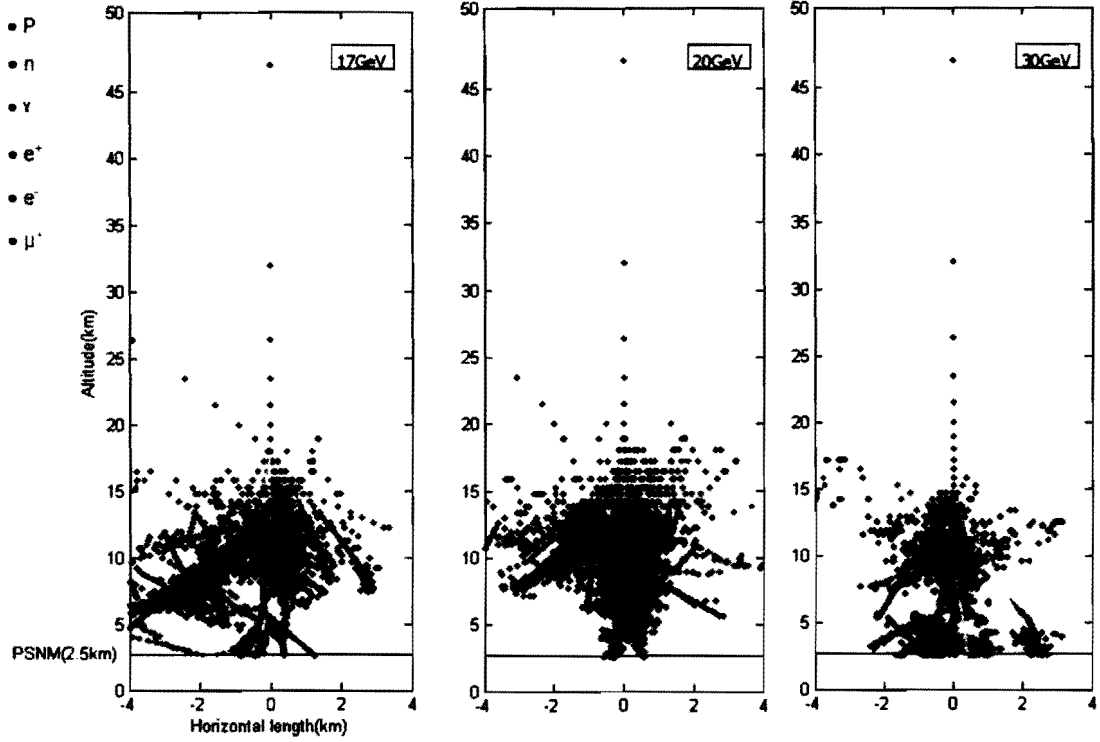


Figure 6.4 Show a more realistic simulation when we take the effect of rock (mainly granite) into account. The PSNM level are shown by a solid line.

6.2 Calculation of neutron flux

The goal of our FLUKA simulations is to calculate the neutron flux at Doi Inthanon's altitude of 2565 meters. These neutrons are secondary particles in the simulation. We define N as the number of neutrons per ($\text{cm}^2\text{-s-GeV}$) and E as the kinetic energy of each neutron to create the following equation:

$$N(E_n) = 2\pi \int_{E_p=17} S(E_n, E_p) j(E_p) dE_p, \quad (6.1)$$

where S is the yield function in units of (neutrons/GeV) per primary proton, E_p and E_n are the kinetic energies of the primary proton and secondary neutron, respectively, 2π is multiplied to account for integration over solid angle for the entire sky, and $j(E_p)$ is the Galactic cosmic ray flux, given by (Nakamura, 2010)

$$j(E_p) = 1.8 \left(\frac{E_p}{1 \text{ GeV}} \right)^{-2.65} \frac{\text{protons}}{\text{cm}^2\text{-s-sr-GeV}}. \quad (6.2)$$

Thus we use FLUKA simulations to derive $S(E_n, E_p)$, and equation 6.1 can then give us $N(E_n)$.

Next, we change equation 6.1 into a summation in order to combine the results of various FLUKA simulations:

$$N(E_n) = 2\pi \sum_{E_p=17} S(E_n, E_p) j(E_p) \Delta E_p, \quad (6.3)$$

where ΔE_p is the interval in primary proton kinetic energy. The summation over E_p starts from 17 GeV, the kinetic energy of vertical primary protons corresponding to the vertical cutoff rigidity at Doi Inthanon.

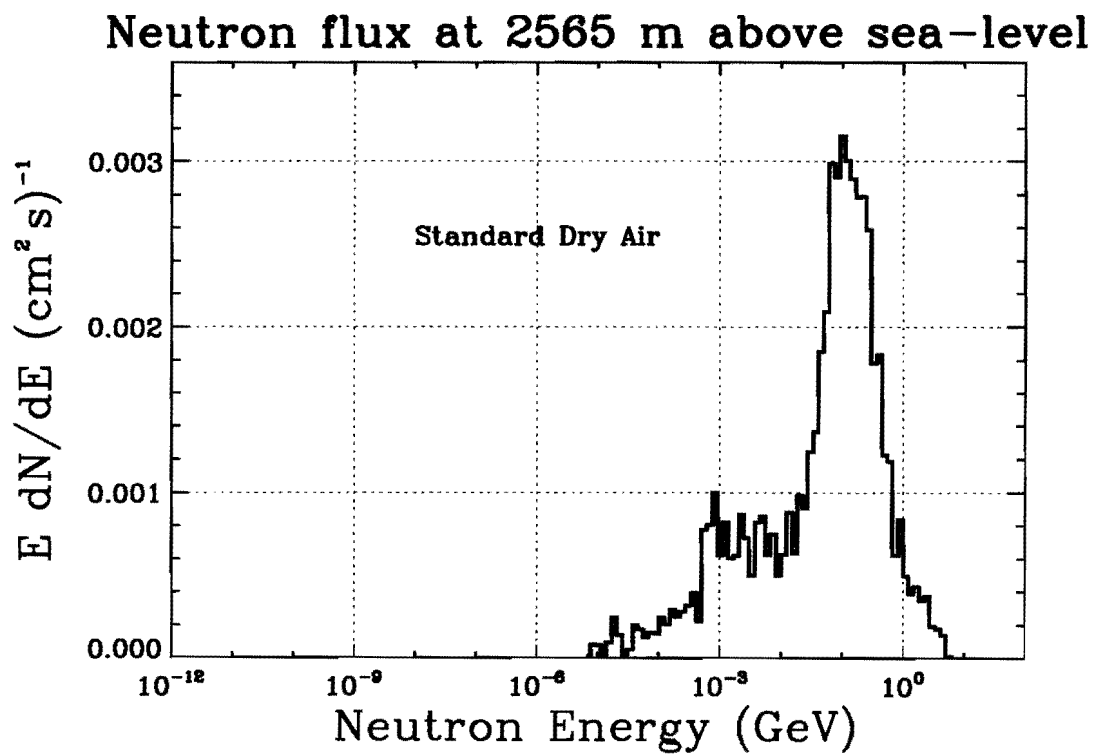


Figure 6.5 Secondary neutron flux at Doi Inthanon's altitude of 2565 meters with dry air

6.3 Including a mountain of rock (granite)

This simulation replaces part of the BLACKHOLE with granite rock for realistic modeling of Doi Inthanon. The resulting low-energy neutron flux (Figure 6.6) is higher than that of Figure 6.5 because some neutrons undergo spallation or reflect and lose their energy at the rock, then spraying upward to form a cloud of low-energy neutrons, which can thermalize and diffuse downward again with lower energy.

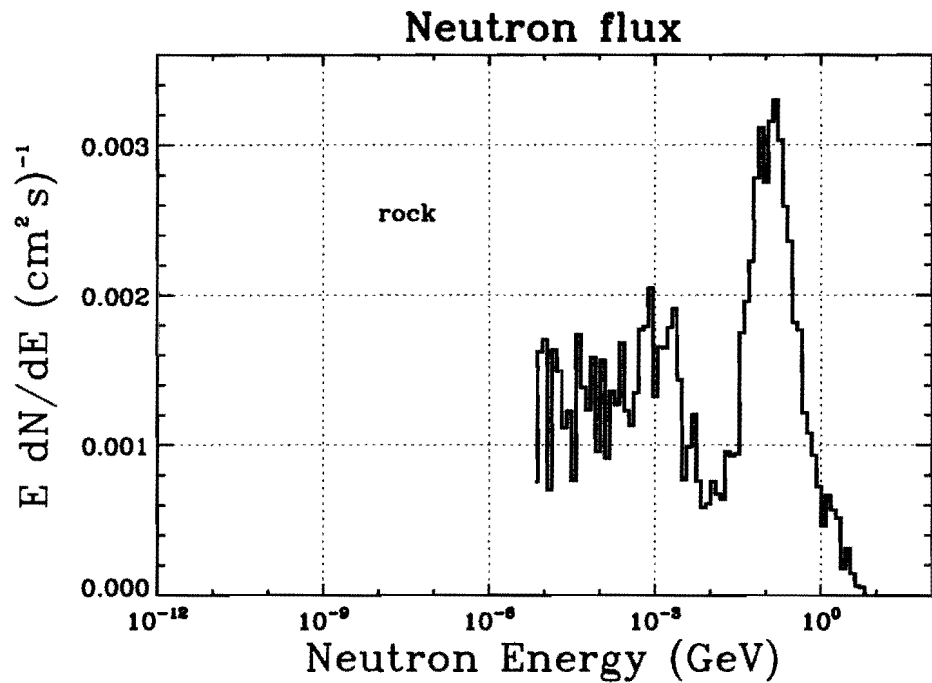


Figure 6.6 Histogram of the flux of neutrons as a function of log (kinetic energy), including the mountain of rock

We also compare the results figure 6.6 with figure 6.7, produced by John Clem from the University of Delaware for the same simulation except for independent geometry modeling. Both results show consistent neutron spectra at 2565 altitude for all energies considered, including a main peak at about 100 MeV and a tail of low-energy neutrons at ~ 1 MeV.

This result can be used to model the PSNM measurements. The sub-GeV neutrons can easily penetrate the reflector and interact in the lead, and thus result in most of our PSNM counts. However, a bare counter with moderator has a count rate that is probably dominated by intermediate-energy neutrons (with enough energy to get through the moderator), especially if

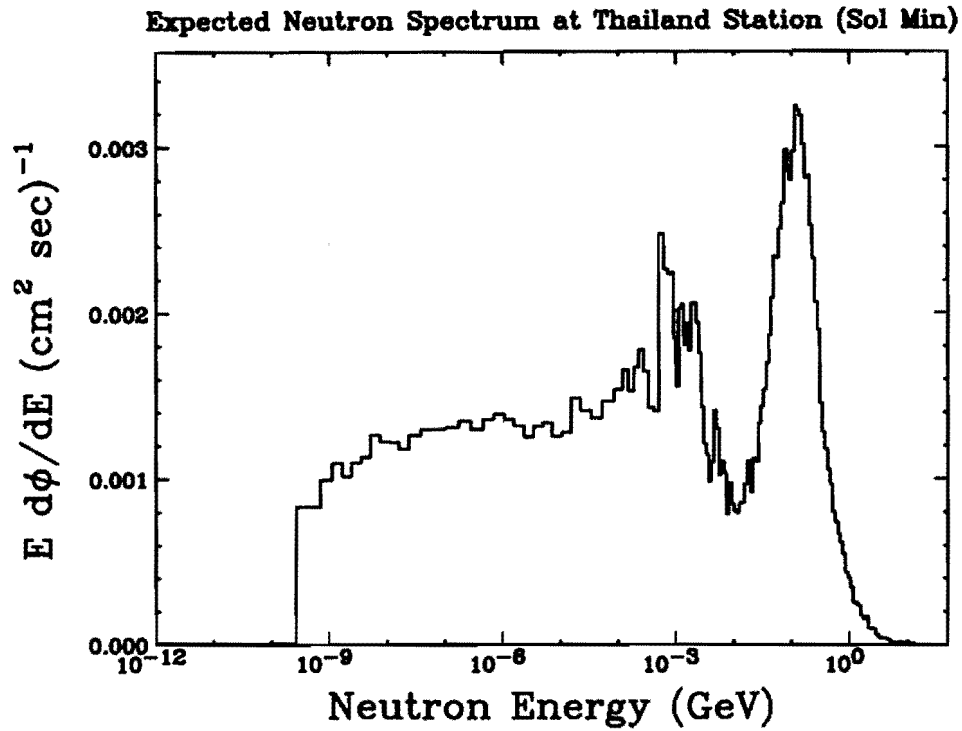


Figure 6.7 Histogram of the flux of neutrons as a function of log (kinetic energy), including the mountain of rock, as generated by John Clem of U. Delaware

they interact with the moderator enough to bounce back and forth across the $^{10}\text{BF}_3$ gas. For the NM64 count rate, the lower-energy neutron tail is not very important. In conclusion, this work we have performed a nucleonic cascade simulation by using FLUKA program. We developed the input files for FLUKA and simulated the effects of the secondary neutrons, on air molecules by taking the effects of rock into account. The results show the expected neutron energy spectrum at Doi Inthanon, that is the neutron produced by atmospheric cascade and could be detected by NM. This work will give us data for further analysis and better understanding of effects of the atmospheric structure on neutron monitor counts. We will also obtain information that can be applied to improve space physics and astrophysics knowledge.

REFERENCES

REFERENCES

- Alvarez, L. and Compton, A. H. "A positively charged component of cosmic rays". Phys. Rev. 10(43): 835, 1934.
- Battistoni, G. and et al. "The FLUKA code: Description and benchmarking", In Proceedings of the Hadronic Shower Simulation Workshop 2006. Raja R., ed. pp. 31-49.
AIP Conference Proceeding: Fermilab, 2007.
- Bradt, H. L. and Peters, B. "Investigation of the Primary Cosmic Radiation with Nuclear Photographic Emulsions", Phys. Rev. 12(74): 1828, 1948.
- Bothe, W. and Kolhörster, W. "Das Wesen der Höhenstrahlung", Zeitschrift für Physik. 56(11): 751-777, 1929.
- Clay, J. Proc. Acad. Wetesch. Amsterdam, 30: 633, 1927.
- Clem, J. M. and Dorman, L. I. "Neutron Monitor Response Functions", Space Science Reviews. 93: 335-359, 2000.
- Clem, J.M. and et al. "Preliminary validation of computational procedures for a new atmospheric ionizing radiation (air) model", Advances in Space Research. 32: 27-33, 2003.
- Ferrari, A. and et al. FLUKA: a multi-particle transport code (Program version 2008). Geneva: CERN, 2005.
- Frier, P. and et al. "Evidence for Heavy Nuclei in the Primary Cosmic Radiation", Phys. Rev. 2(74): 213, 1948.
- Goldhagen, P. and et al. "Measurement of the energy spectrum of cosmic-ray induced neutrons aboard an ER-2 high-altitude airplane", Nuclear Instruments and Methods in Physics Research. A476: 42-51, 2002.
- Hess, V.F. "Über die Beobachtung der durchdringenden Strahlung bei sieben Freiballonfahrten", Z. Phys. 13: 1084, 1912.
- Johnson, T.H. "The Azimuthal Asymmetry of the Cosmic Radiation", Phys. Rev. 10(43): 834, 1934.
- Krane, K. S. Introductory Nuclear Physics. New York: John Wiley and Son, 1988.

REFERENCES (CONTINUE)

- Leerunnavarat, K., Ruffolo, D. and Bieber, J. W. "Loss Cone Precursors to Forbush Decreases and Advance Warning of Space Weather Effects", Astrophysical Journal. 593: 587-596, 2003.
- Metropolis, N. "THE BEGINNING of the MONTE CARLO METHOD", Los Alamos Science Special Issue. 125-130, 1987.
- Nakamura, K. "Review of Particle Physics", Journal of Physics G: Nuclear and Particle Physics. 37: 269, 2010.
- Nattapong Kamyan. Secondary Neutrons from Cosmic Rays in Earth's Atmosphere above the Princess Sirindhorn Neutron Monitor. Master's Thesis: Mahidol University, 2010.
- NOAA, NASA and USAF. U.S. Standard Atmosphere, 1976. Washington, D.C: U.S. Government Printing Office, 1976.
- Pomerantz, M.A. Cosmic Rays. New york: Van Nostrand Reinhold Company, 1971.
- Rossi, B. "On the Magnetic Deflection of Cosmic Rays", Phys. Rev. 3(36): 606, 1930.
- "Directional Measurements on the Cosmic Rays Near the Geomagnetic Equator", Phys. Rev. 3(45): 212, 1934a.
- "Misure della distribuzione angolare di intensita della radiazione penetrare all'Asmara", Ric. Sci. 5(1): 579, 1934b.
- Ruffolo, D. "Transport and Acceleration of Energetic Charged Particles near an Oblique Shock", Astrophysical Journal. 515: 787-800, 1999.
- Sandström, A.E. Cosmic Ray Physics. Amsterdam: North-Holland publishing company, 1965.
- Shellard, R.C. "Cosmic Accelerator and Terrestrial Detectors ", Brazilian Journal of Physics. 2(31): 247, 2001.
- Tibor, J.D. Cosmogenic Nuclides : Principles, Concepts and Applications in the Earth Surface Sciences. United Kingdom: Cambridge University Press, 2010.

APPENDICES

APPENDIX A

MODEL OF ATMOSPHERIC PROPERTIES

The table A.1 shows information regarding each layer of our model of the atmosphere for FLUKA simulations. The columns in the table are as follows:

- | | |
|---|--|
| 1. Layer number (i) | 6. Altitude at the top (z_t) in cm |
| 2. Pressure at the bottom (P_b) in Pa | 7. Density (ρ) in kg/m ² |
| 3. Pressure at the top (P_t) in Pa | 8. Temperature at the bottom (T_b) in K |
| 4. Reference pressure (P_{ref}) in Pa | 9. Temperature at the top (T_t) in K |
| 5. Altitude at the bottom (z_b) in cm | 10. Reference temperature (T_{ref}) in K |

Table A.1. Values in the FLUKA input file “AtmosphereInf.txt”

<i>i</i>	P_b (pascals)	P_t (pascals)	P_{ref} (pascals)	z_b (cm)	z_t (cm)	ρ (kg/m ²)	T_b (K)	T_t (K)	T_{ref} (K)
1	101325.0000	100303.0143	100814.0071	0.000e+000	8.542e+003	1.220e+000	288.15	287.59	287.87
2	100303.0143	99281.0286	99792.0214	8.542e+003	1.716e+004	1.210e+000	287.59	287.03	287.31
3	99281.0286	98259.0429	98770.0357	1.716e+004	2.584e+004	1.200e+000	287.03	286.47	286.75
4	98259.0429	97237.0571	97748.0500	2.584e+004	3.460e+004	1.190e+000	286.47	285.90	286.19
5	97237.0571	96215.0714	96726.0643	3.460e+004	4.343e+004	1.180e+000	285.90	285.33	285.61
6	96215.0714	95193.0857	95704.0786	4.343e+004	5.234e+004	1.170e+000	285.33	284.75	285.04
7	95193.0857	94171.1000	94682.0929	5.234e+004	6.133e+004	1.160e+000	284.75	284.16	284.46
8	94171.1000	93149.1143	93660.1071	6.133e+004	7.040e+004	1.149e+000	284.16	283.57	283.87
9	93149.1143	92127.1286	92638.1214	7.040e+004	7.954e+004	1.139e+000	283.57	282.98	283.28
10	92127.1286	91105.1429	91616.1357	7.954e+004	8.877e+004	1.129e+000	282.98	282.38	282.68
11	91105.1429	90083.1571	90594.1500	8.877e+004	9.809e+004	1.119e+000	282.38	281.77	282.08
12	90083.1571	89061.1714	89572.1643	9.809e+004	1.075e+005	1.109e+000	281.77	281.16	281.47
13	89061.1714	88039.1857	88550.1786	1.075e+005	1.170e+005	1.098e+000	281.16	280.55	280.85
14	88039.1857	87017.2000	87528.1929	1.170e+005	1.266e+005	1.088e+000	280.55	279.92	280.24
15	87017.2000	85995.2143	86506.2071	1.266e+005	1.362e+005	1.078e+000	279.92	279.30	279.61
16	85995.2143	84973.2286	85484.2214	1.362e+005	1.460e+005	1.067e+000	279.30	278.66	278.98

Table A.1. Values in the FLUKA input file “AtmosphereInf.txt” (cont.)

i	P_b (pascals)	P_t (pascals)	P_{ref} (pascals)	z_b (cm)	z_t (cm)	ρ (kg/m ³)	T_b (K)	T_t (K)	T_{ref} (K)
17	84973.2286	83951.2429	84462.2357	1.460e+005	1.558e+005	1.057e+000	278.66	278.02	278.34
18	83951.2429	82929.2571	83440.2500	1.558e+005	1.658e+005	1.047e+000	278.02	277.37	277.70
19	82929.2571	81907.2714	82418.2643	1.658e+005	1.759e+005	1.036e+000	277.37	276.72	277.05
20	81907.2714	80885.2857	81396.2786	1.759e+005	1.860e+005	1.026e+000	276.72	276.06	276.39
21	80885.2857	79863.3000	80374.2929	1.860e+005	1.963e+005	1.015e+000	276.06	275.39	275.73
22	79863.3000	78841.3143	79352.3071	1.963e+005	2.066e+005	1.005e+000	275.39	274.72	275.05
23	78841.3143	77819.3286	78330.3214	2.066e+005	2.171e+005	9.945e-001	274.72	274.04	274.38
24	77819.3286	76797.3429	77308.3357	2.171e+005	2.277e+005	9.840e-001	274.04	273.35	273.69
25	76797.3429	75775.3571	76286.3500	2.277e+005	2.384e+005	9.735e-001	273.35	272.65	273.00
26	75775.3571	74753.3714	75264.3643	2.384e+005	2.492e+005	9.629e-001	272.65	271.95	272.30
27	74753.3714	73731.3857	74242.3786	2.492e+005	2.602e+005	9.523e-001	271.95	271.24	271.59
28	73731.3857	72709.4000	73220.3929	2.602e+005	2.713e+005	9.416e-001	271.24	270.52	270.88
29	72709.4000	71687.4143	72198.4071	2.713e+005	2.824e+005	9.310e-001	270.52	269.79	270.15
30	71687.4143	70665.4286	71176.4214	2.824e+005	2.938e+005	9.203e-001	269.79	269.05	269.42
31	70665.4286	69643.4429	70154.4357	2.938e+005	3.052e+005	9.096e-001	269.05	268.31	268.68
32	69643.4429	68621.4571	69132.4500	3.052e+005	3.168e+005	8.988e-001	268.31	267.56	267.93

Table A.1. Values in the FLUKA input file “AtmosphereInf.txt” (cont.)

i	P_b (pascals)	P_t (pascals)	P_{ref} (pascals)	z_b (cm)	z_t (cm)	ρ (kg/m ³)	T_b (K)	T_t (K)	T_{ref} (K)
33	68621.4571	67599.4714	68110.4643	3.168e+005	3.286e+005	8.881e-001	267.56	266.79	267.17
34	67599.4714	66577.4857	67088.4786	3.286e+005	3.404e+005	8.773e-001	266.79	266.02	266.41
35	66577.4857	65555.5000	66066.4929	3.404e+005	3.525e+005	8.664e-001	266.02	265.24	265.63
36	65555.5000	64533.5143	65044.5071	3.525e+005	3.646e+005	8.556e-001	265.24	264.45	264.84
37	64533.5143	63511.5286	64022.5214	3.646e+005	3.770e+005	8.447e-001	264.45	263.65	264.05
38	63511.5286	62489.5429	63000.5357	3.770e+005	3.895e+005	8.337e-001	263.65	262.83	263.24
39	62489.5429	61467.5571	61978.5500	3.895e+005	4.022e+005	8.228e-001	262.83	262.01	262.42
40	61467.5571	60445.5714	60956.5643	4.022e+005	4.150e+005	8.118e-001	262.01	261.18	261.59
41	60445.5714	59423.5857	59934.5786	4.150e+005	4.280e+005	8.007e-001	261.18	260.33	260.75
42	59423.5857	58401.6000	58912.5929	4.280e+005	4.412e+005	7.896e-001	260.33	259.47	259.90
43	58401.6000	57379.6143	57890.6071	4.412e+005	4.546e+005	7.785e-001	259.47	258.60	259.04
44	57379.6143	56357.6286	56868.6214	4.546e+005	4.682e+005	7.674e-001	258.60	257.72	258.16
45	56357.6286	55335.6429	55846.6357	4.682e+005	4.820e+005	7.562e-001	257.72	256.82	257.27
46	55335.6429	54313.6571	54824.6500	4.820e+005	4.959e+005	7.450e-001	256.82	255.91	256.37
47	54313.6571	53291.6714	53802.6643	4.959e+005	5.101e+005	7.337e-001	255.91	254.99	255.45
48	53291.6714	52269.6857	52780.6786	5.101e+005	5.246e+005	7.224e-001	254.99	254.05	254.52

Table A.1. Values in the FLUKA input file “AtmosphereInf.txt” (cont.)

i	P_b (pascals)	P_t (pascals)	P_{ref} (pascals)	z_b (cm)	z_t (cm)	ρ (kg/m ³)	T_b (K)	T_t (K)	T_{ref} (K)
49	52269.6857	51247.7000	51758.6929	5.246e+005	5.392e+005	7.110e-001	254.05	253.10	253.58
50	51247.7000	50225.7143	50736.7071	5.392e+005	5.541e+005	6.997e-001	253.10	252.13	252.62
51	50225.7143	49203.7286	49714.7214	5.541e+005	5.693e+005	6.882e-001	252.13	251.15	251.64
52	49203.7286	48181.7429	48692.7357	5.693e+005	5.847e+005	6.767e-001	251.15	250.15	250.65
53	48181.7429	47159.7571	47670.7500	5.847e+005	6.003e+005	6.652e-001	250.15	249.13	249.64
54	47159.7571	46137.7714	46648.7643	6.003e+005	6.163e+005	6.536e-001	249.13	248.09	248.61
55	46137.7714	45115.7857	45626.7786	6.163e+005	6.325e+005	6.420e-001	248.09	247.04	247.56
56	45115.7857	44093.8000	44604.7929	6.325e+005	6.490e+005	6.304e-001	247.04	245.96	246.50
57	44093.8000	43071.8143	43582.8071	6.490e+005	6.659e+005	6.186e-001	245.96	244.87	245.42
58	43071.8143	42049.8286	42560.8214	6.659e+005	6.831e+005	6.069e-001	244.87	243.75	244.31
59	42049.8286	41027.8429	41538.8357	6.831e+005	7.006e+005	5.950e-001	243.75	242.61	243.18
60	41027.8429	40005.8571	40516.8500	7.006e+005	7.184e+005	5.831e-001	242.61	241.45	242.03
61	40005.8571	38983.8714	39494.8643	7.184e+005	7.367e+005	5.712e-001	241.45	240.27	240.86
62	38983.8714	37961.8857	38472.8786	7.367e+005	7.553e+005	5.592e-001	240.27	239.05	239.66
63	37961.8857	36939.9000	37450.8929	7.553e+005	7.744e+005	5.471e-001	239.05	237.82	238.44
64	36939.9000	35917.9143	36428.9071	7.744e+005	7.938e+005	5.350e-001	237.82	236.55	237.18

Table A.1. Values in the FLUKA input file “AtmosphereInf.txt” (cont.)

i	P_b (pascals)	P_t (pascals)	P_{ref} (pascals)	z_b (cm)	z_t (cm)	ρ (kg/m ³)	T_b (K)	T_t (K)	T_{ref} (K)
65	35917.9143	34895.9286	35406.9214	7.938e+005	8.138e+005	5.228e-001	236.55	235.25	235.90
66	34895.9286	33873.9429	34384.9357	8.138e+005	8.342e+005	5.106e-001	235.25	233.93	234.59
67	33873.9429	32851.9571	33362.9500	8.342e+005	8.551e+005	4.983e-001	233.93	232.57	233.25
68	32851.9571	31829.9714	32340.9643	8.551e+005	8.766e+005	4.859e-001	232.57	231.17	231.87
69	31829.9714	30807.9857	31318.9786	8.766e+005	8.986e+005	4.734e-001	231.17	229.74	230.46
70	30807.9857	29786.0000	30296.9929	8.986e+005	9.212e+005	4.608e-001	229.74	228.27	229.01
71	29786.0000	28764.0143	29275.0071	9.212e+005	9.444e+005	4.482e-001	228.27	226.76	227.52
72	28764.0143	27742.0286	28253.0214	9.444e+005	9.684e+005	4.355e-001	226.76	225.21	225.98
73	27742.0286	26720.0429	27231.0357	9.684e+005	9.930e+005	4.227e-001	225.21	223.60	224.41
74	26720.0429	25698.0571	26209.0500	9.930e+005	1.018e+006	4.098e-001	223.60	221.95	222.78
75	25698.0571	24676.0714	25187.0643	1.018e+006	1.045e+006	3.968e-001	221.95	220.24	221.10
76	24676.0714	23654.0857	24165.0786	1.045e+006	1.072e+006	3.837e-001	220.24	218.48	219.36
77	23654.0857	22632.1000	23143.0929	1.072e+006	1.100e+006	3.705e-001	218.48	216.65	217.56
78	22632.1000	21622.8524	22127.4762	1.100e+006	1.129e+006	3.557e-001	216.65	216.65	216.65
79	21622.8524	20613.6047	21118.2285	1.129e+006	1.159e+006	3.395e-001	216.65	216.65	216.65
80	20613.6047	19604.3571	20108.9809	1.159e+006	1.191e+006	3.233e-001	216.65	216.65	216.65

Table A.1. Values in the FLUKA input file “AtmosphereInf.txt” (cont.)

i	P_b (pascals)	P_t (pascals)	P_{ref} (pascals)	z_b (cm)	z_t (cm)	ρ (kg/m ²)	T_b (K)	T_t (K)	T_{ref} (K)
81	19604.3571	18595.1094	19099.7332	1.191e+006	1.225e+006	3.070e-001	216.65	216.65	216.65
82	18595.1094	17585.8618	18090.4856	1.225e+006	1.260e+006	2.908e-001	216.65	216.65	216.65
83	17585.8618	16576.6141	17081.2379	1.260e+006	1.297e+006	2.746e-001	216.65	216.65	216.65
84	16576.6141	15567.3665	16071.9903	1.297e+006	1.337e+006	2.583e-001	216.65	216.65	216.65
85	15567.3665	14558.1188	15062.7426	1.337e+006	1.380e+006	2.421e-001	216.65	216.65	216.65
86	14558.1188	13548.8712	14053.4950	1.380e+006	1.425e+006	2.259e-001	216.65	216.65	216.65
87	13548.8712	12539.6235	13044.2474	1.425e+006	1.474e+006	2.096e-001	216.65	216.65	216.65
88	12539.6235	11530.3759	12034.9997	1.474e+006	1.528e+006	1.934e-001	216.65	216.65	216.65
89	11530.3759	10521.1282	11025.7521	1.528e+006	1.586e+006	1.772e-001	216.65	216.65	216.65
90	10521.1282	9511.8806	10016.5044	1.586e+006	1.650e+006	1.609e-001	216.65	216.65	216.65
91	9511.8806	8502.6329	9007.2568	1.650e+006	1.721e+006	1.447e-001	216.65	216.65	216.65
92	8502.6329	7493.3853	7998.0091	1.721e+006	1.801e+006	1.284e-001	216.65	216.65	216.65
93	7493.3853	6484.1376	6988.7615	1.801e+006	1.893e+006	1.122e-001	216.65	216.65	216.65
94	6484.1376	5474.8900	5979.5138	1.893e+006	2.000e+006	9.592e-002	216.65	216.65	216.65
95	5474.8900	4323.1723	4899.0311	2.000e+006	2.150e+006	7.814e-002	216.65	218.15	217.40
96	4323.1723	3171.4545	3747.3134	2.150e+006	2.349e+006	5.910e-002	218.15	220.14	219.15

Table A.1. Values in the FLUKA input file “AtmosphereInf.txt” (cont.)

i	P_b (pascals)	P_t (pascals)	P_{ref} (pascals)	z_b (cm)	z_t (cm)	ρ (kg/m ²)	T_b (K)	T_t (K)	T_{ref} (K)
97	3171.4545	2019.7368	2595.5956	2.349e+006	2.642e+006	4.013e-002	220.14	223.07	221.60
98	2019.7368	868.0190	1443.8779	2.642e+006	3.200e+006	2.104e-002	223.07	228.65	225.86
99	868.0190	110.9060	489.4625	3.200e+006	4.700e+006	5.147e-003	228.65	270.65	249.65
100	110.9060	66.9389	88.9224	4.700e+006	5.100e+006	1.121e-003	270.65	270.65	270.65

APPENDIX B

PRESSURE AND DENSITY EQUATIONS

This Appendix shows a derivation of the pressure and density equations in Chapter 4, using the ideal gas law,

$$P = \frac{\rho RT}{M}, \quad (\text{B.1})$$

and hydrostatic equilibrium,

$$dP = -\rho g dz \quad (\text{B.2})$$

We divide equation B.2 by equation B.1:

$$\frac{dP}{P} = -\frac{gM dz}{RT} \quad (\text{B.3})$$

Integrating equation B.3 from h_b to h in altitude and P_b to P in pressure, we obtain

$$\int_{P_b}^P \frac{dP'}{P'} = - \int_{h_b}^h \frac{gM dz}{RT} \quad (\text{B.4})$$

In the case of constant T (lapse rate $L_b=0$), we have

$$\ln \left(\frac{P}{P_b} \right) = -\frac{gM}{RT} (h - h_b) \quad (\text{B.5})$$

$$P = P_b e^{-gM(h-h_b)/RT} \quad (\text{B.6})$$

In the case that T changes with the lapse rate L_b ,

$$T = T_b + (h - h_b)L_b, \quad (\text{B.7})$$

and

$$dT = L_b dz \quad (\text{B.8})$$

We replace dz in equation B.4 and integrate the temperature from T_b to T :

$$\int_{P_b}^P \frac{dP'}{P'} = - \int_{T_b}^T \frac{gM}{L_b R} \left(\frac{dT'}{T'} \right) \quad (\text{B.9})$$

$$\ln \left(\frac{P}{P_b} \right) = - \frac{gM}{L_b R} \ln \left(\frac{T}{T_b} \right) \quad (\text{B.10})$$

$$\frac{P}{P_b} = \left(\frac{T}{T_b} \right)^{-\frac{gM}{L_b R}} \quad (\text{B.11})$$

We replace T with equation B.7:

$$P = P_b \left(\frac{T_b + (h - h_b) L_b}{T_b} \right)^{-\frac{gM}{L_b R}} \quad (\text{B.12})$$

$$P = P_b \left(\frac{T_b}{T_b + (h - h_b) L_b} \right)^{\frac{gM}{L_b R}}, \quad (\text{B.13})$$

so we get,

$$P = P_b \cdot \left[\frac{T_b}{T_b + L_b(h - h_b)} \right]^{\frac{g \cdot M}{R \cdot L_b}} \quad \text{if } L_b \neq 0, \quad (\text{B.14})$$

$$P = P_b \cdot \exp \left[\frac{-g \cdot M \cdot (h - h_b)}{R \cdot T_b} \right] \quad \text{if } L_b = 0 \quad (\text{B.15})$$

For the density equation, we define the density formula as follows:

$$\rho_b \equiv \frac{1}{h_{b+1} - h_b} \int_{h_b}^{h_{b+1}} \rho(z) \cdot dz. \quad (\text{B.16})$$

From the hydrostatic equilibrium equation B.2,

$$\rho dz = -\frac{dP}{g} \quad (\text{B.17})$$

We replace ρdz in equation B.16 with equation B.17 and integrate the pressure from P_b to P_{b+1} :

$$\rho_b = \frac{1}{h_{b+1} + h_b} \int_{P_b}^{P_{b+1}} -\frac{dP'}{g} \quad (\text{B.18})$$

By integrating equation B.18, we obtain

$$\rho_b = -\frac{P_{b+1} - P_b}{g \cdot (h_{b+1} - h_b)} \quad (\text{B.19})$$

VITAE

NAME	Mr.Dumrongsak Rodphothong
INSTITUTIONS ATTENDED	Kasetsart University, 2003-2007 Bachelor of Science (Physics) Ubon Ratchathani University, 2009-2012 Master of Science (Physics)
SCHOLARSHIPS	Research assistant, Thailand Center of Excellence in Physics, 2010
HOME ADDRESS	160 Satonramak Road Warincumrab, Ubon Ratchathani Thailand, 34190
E-MAIL	dumrongsak_r@hotmail.com